Optomechanics for Gravitational Wave Detection — from resonant bars to next generation laser interferometers

David Blair, Li Ju and Yiqiu Ma
School of Physics, The University of Western Australia

OXFORD
UNIVERSITY PRESS

Acknowledgements

This paper reviews 40 years of research that includes enormous contributions by many PhD students and postdocs at UWA as well as international colleagues. Robin Giffard, Vladimir Braginsky and Bill Hamilton made enormous contributions to the fundamental ideas. Underpinning the research at UWA was the outstanding UWA Physics Workshop where highly skilled technicians made enormous contributions. Ron Bowers, John Devlin, Arthur Woods, Steve Popel, John Moore and Peter Hay made enormous contributions to the construction of bar detector NIOBE and/or to the construction of the 80m interferometer at the Gingin research centre. John Ferreirinho, Tony Mann, Peter Veitch, Peter Turner, Steve Jones, Eugene Ivanov, Mike Tobar ,Ik Siong Heng and Nick Linthorne made enormous contributions to the success of NIOBE, and Peng Hong, Mitsuru Taniwaki and Brett Cuthbertson made huge contributions to transducer development. John Winterflood, Jean-Charles Dumas, Ben Lee and Eu-jeen Chin built the vibration isolators that underpinned all the research at Gingin. Mark Nottcut helped us develop interferometry at UWA. Chunnong Zhao built the first interferometer and designed almost all the important experiments at Gingin. Slawek Gras, Pablo Barriga and Jerome Degallix did all the heavy lifting for understanding parametric instability,thermal tuning and cavity mode structures. Yaohui Fan, Sunil Sunsmithan, Qi Fang, and Carl Blair undertook enormously difficult experiments at Gingin while Xu (Sundae) Chen and Jiayi Qin undertook the very difficult small scale experiments. Haixing Miao, and Stefan Danilishin made enormous contributions to our understanding of quantum optomechanics. We owe our thanks to many many others whose names are not listed here.

Contents

1

Optomechanics for Gravitational Wave Detection - from resonant bars to next generation laser interferometers

1.1 Introduction

This paper is written at the time of the first direct detection of gravitational waves, one century after the gravitational wave spectrum was first predicted and fifty years after physicists first began to design and construct instruments for this purpose. The discovery was made by the Advanced LIGO detectors which themselves are masterpieces of optomechanical physics and engineering. The detectors are a culmination of half a century of innovation, during which the principles and the technologies of ultrasensitive mechanical measurements were developed, in particular through the development of optomechanics, pioneered by physicists developing earlier generations of gravitational wave detectors.

In 2015 the Advanced LIGO detectors had achieved a factor of $3-4$ improvement in amplitude sensitivity. This small step took us across a threshold, from inability to detect astronomical signals, to a regime in which strong signals have become detectable. The next steps in sensitivity will offer enormous scientific rewards.

This paper reviews the 40 year history that led to the first detection of gravitational waves, and goes on to outline techniques which will allow the detectors to be substantially improved. Following a review of the gravitational wave spectrum and the early attempts at detection, it emphasises the theme of optomechanics, and the underlying physics of parametric transducers, which was creates a connection between early resonant bar detectors and modern interferometers and techniques for enhancing their sensitivity.

Developments are presented in an historical context, while themes and connections between earlier and later work are emphasised. We begin by reviewing the gravitational wave spectrum.

1.2 The Gravitational Wave Spectrum

Nature provides us with two fundamental spectrums of zero rest mass wave-like excitations which travel through empty space at the speed of light. The spectrum of electromagnetic waves was predicted by James Clerk Maxwell in 1865 (Maxwell, 1865),

150 years before this Les Houches summer school. It was more than 2 decades before Heinrich Hertz (Hertz, 1887) succeeded in generating and detecting Maxwell's waves. At the turn of the 20th century Marconi and others created radios, but it took another century of innovation to fully harness Maxwell's spectrum, from the lowest frequencies, such as the Schumann resonances of the Earth's ionosphere, for which the photons have energy $\sim 10^{-32}$ J to the highest energy gamma rays, for which the photon energy approaches 1 Joule.

Fifty years after Maxwell published his electromagnetic field equations, Einstein published the field equations of General Relativity. As shown by Einstein in 1916 and 1918 (Einstein, 1916; Einstein, 1918) the equations predicted gravitational waves which are ripples in spacetime described by the Reimann tensor. Einstein considered the waves to be of academic interest only, because their effects appeared to be too small to measure. Others even suggested that the waves were mathematical artifacts. It was not until 1957 that the theoretical case was made for gravitational waves having firm physical reality, with ability to transport energy and do work. This was demonstrated in a thought experiment by Richard Feynman at a conference in Chapel Hill (Rickles and DeWitt, 2011), that marked the beginning of the modern resurgence of General Relativity.

Even though gravitational waves have firm physical reality, their detection is a daunting challenge because the interaction of gravitational waves with matter is very weak. In this section we will use simple arguments to estimate the amplitude and frequency of gravitational waves. Wave amplitude is measured in dimensionless units that characterise the spatial strain amplitude, that represent the fluctuating spacing $\triangle L$ between inertial test masses spaced distance L apart: $h = \Delta L/L$.

In their most compact form, Einstein's equations can be written as $\mathbf{G} = (8\pi G/c^4)\mathbf{T}$, where $\mathbf{G}$ is the Einstein curvature tensor which describes the curvature of spacetime and $\mathbf{T}$ is the stress energy tensor that describes the mass-energy distribution. The coupling constant $8\pi G/c^4$ has a magnitude $\sim 10^{-43}$. Time varying stress-energy creates waves of curvature which can be measured as a strain h. Without deriving the wave equation (which can be found in numerous sources) it is obvious that the curvature fluctuations in general must have small amplitude because of the smallness of the coupling constant.

In 1916 Schwarzschild published a solution for Einsteins field equations in the limit of spherical symmetry. His solution describes the spacetime of black holes for which there is a central singularity and an event horizon, of radius now known as the Schwartzchild radius, given by $r_s = 2GM/c^2$. At this time there was no evidence for the physical reality of black holes.

The spacetime curvature for a gravitating source of mass M can be estimated from the ratio of r_s/r. For the Earth $r_s/r < 10^{-8}$ where r is the radius of the Earth. At the surface of the Sun, $r_s/r \sim 10^{-6}$. These small factors show that general relativistic effects including the generation of gravitational waves are extremely weak in the solar system.

Einstein showed that the gravitational wave luminosity of a source depends approximately on the square of the third time derivative of the quadrupole moment of the source. The simplest source is a pair of masses orbiting each other. For equal

masses M orbiting each other at distance L apart and with orbital frequency ω, the gravitational wave luminosity $L_{\rm G}$ is given (neglecting constants ~ 1) by

$$L_{\rm G} \sim \frac{G}{c^5} M^2 L^4 \omega^6. \tag{1.1}$$

The same formula can be expressed in terms appropriate for a binary pair of black holes. In this case it resolves to

$$L_{\rm G} \sim \frac{c^5}{G} (\frac{v}{c})^6 (\frac{r_{\rm s}}{r})^2. \tag{1.2}$$

Here the gravitational wave luminosity depends only on the scale r of the system relative to the Schwarzschild radius, and the velocity of the two masses compared to the speed of light.

Equation 1.2 is remarkably different from equation 1.1. The coupling factor has been inverted, so that the gravitational wave power emitted is now scaled by the enormous factor c^5/G, which has magnitude $\sim 10^{53}$. Since two black holes will merge with velocity $v \sim c$ at a spacing $2r \sim 2r_s$, it follows that black hole coalescence can create enormous gravitational wave luminosity $\sim 10^{53}$ Watts, 10^{23} times the solar luminosity. This power output is independent of the system mass. Because the event duration is directly proportional to mass, the total energy output increases with mass. Numerical calculations (Pretorius, 2005) show that the above estimates are roughly correct.

A binary black hole coalescence creates the most powerful energy outbursts since the big bang. Typically (depending on the black hole spins and mass ratio) it emits about 5% of the system rest mass in gravitational waves. For this reason such systems have always ranked high amongst the targets of gravitational wave astronomy, but lack of knowledge about formation processes for such systems meant that there was always large uncertainty about the event rate for such coalescences. The first detection represented a gravitational explosion of 3 solar masses of energy, the most powerful transient astronomical event ever observed.

It is easy to use intuitive arguments to estimate the amplitude and frequency of gravitational waves from black hole binary coalescence. To estimate amplitude we use the fact that the spatial perturbations will be maximal at distance $\sim r_{\rm s}$ from the source at the moment of final merger. At this point, where the curvature is so strong that light paths can be deflected by almost 2π radians, and simultaneously are modulated by the dynamical motion of the black holes, the strain amplitude h reaches a maximal value ~ 1. The escaping waves reduce in amplitude inversely with distance such that the wave intensity (proportional to amplitude squared) follows the usual inverse square law. Thus for coalescence of equal mass black holes the peak amplitude of the waves at the Earth is roughly given by $r_{\rm s}/R$ where $r_{\rm s}$ again represents the black hole Schwarzschild radius and R is the distance between the source and the Earth.

For the coalescence of supermassive black holes of mass $10^9 M_{\rm sun}$, at cosmological distances (say 10^{26} meters or 10 billion light years), the amplitude at Earth would be about 10^{-15}. For 30 solar mass black holes, at 10^{25} meters distance, the amplitude would be 10^{-20}. These numbers are upper limits, because the naive estimate ignores

the relativistic corrections to the source dynamics, and ignores the gravitational red shift of the escaping gravitational waves.

Since the Schwarzschild radius depends linearly on mass, it follows that the gravitational wave frequency for binary black hole coalescence depends inversely on the system mass. The peak frequency of the gravitational waves is determined roughly by the orbital period of the last stable orbit ($3r_s$). For $10^9 M_{sun}$ black holes this radius $\sim 10^{13}$ meters corresponds to a frequency $\sim 10^{-5}$ Hz or one cycle per day. For stellar mass black holes, say $30M_{sun}$, $r_s \sim 10^5$ meters and the peak frequency is a few hundred Hz.

Today we have broad understanding of the expected gravitational wave spectrum. It is summarised in Fig. 1.1. Detectable sources are predicted from 10^{-18} Hz to $\sim 10^4$ Hz, as well as speculative sources at even higher frequency. There are four frequency bands in which there are significant detection efforts. In the cosmological frequency band below 10^{-16}Hz, frozen relic gravitational waves from the big bang should create a polarisation signature in the cosmic microwave background. Claims of detection in this band in 2014 have been shown as likely to be due to foreground dust (Ade *et al.*, 2015), but future multi-frequency observations may be able to separate dust from the gravitational waves, thereby enabling the testing of theories of inflation. In the nanohertz frequency band, gravitational waves created by supermassive black hole binaries (prior to merger) are potential sources. These could be detected as correlated perturbations in the arrival times of pulses from millisecond pulsars. Detection could allow the growth history of supermassive black holes to be measured.

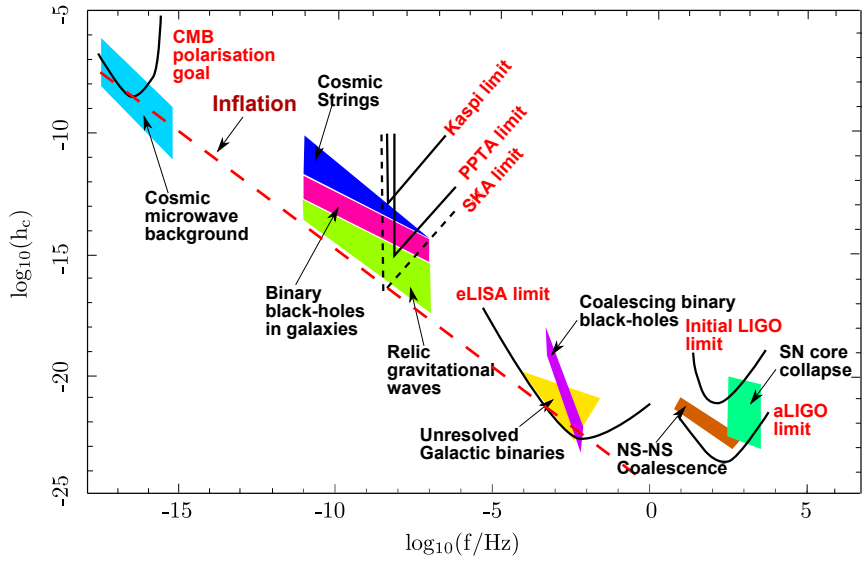

Fig. 1.1 An outline of the expected spectrum of gravitational waves and detection techniques. The spectrum spans 20 decades, from frozen relic waves at 10^{-16} Hz to the audio frequency band.

At millihertz frequencies, gravitational waves from objects falling into intermediate mass black holes, and binary stars systems in the Milky Way are likely to be detectable by future multimillion-km space based laser interferometers.

This paper focuses on the optomechanics for gravitational wave detection in the audio frequency band. This is the best developed frequency band, offering a rich variety of sources. See reference (Blair *et al.*, 2012) for a detailed discussion of the range of potential sources. The Advanced LIGO and Advanced Virgo gravitational wave detectors were specifically designed to target the coalescence of binary neutron stars because these are a known population with a moderately well predicted event rate.

Since binary black holes had never been observed until the recent detection, the event rate for binary black hole coalescence could only be estimated through astrophysical modelling. They are likely to have originated from very massive Population III stars in the early universe. There are two ways they could have been created. They could have been born from a high mass Population III binary pair, that evolved rapidly to become black holes. The initial orbital separation of the binary black hole system determines the lifetime to coalescence. If the separation is too large, the time to coalescence can greatly exceed the age of the universe. Observations of coalescence events select for systems born with suitable initial separations.

A more likely source of binary black holes that can be observed merging today, consist of binaries created inside globular clusters. Modelling shows that isolated black holes born from Population III stars in the early universe are likely to sink towards the cores of globular clusters and also into the high density cusps in the centre of galaxies. Here black hole binaries are likely to be formed by capture events,interactions with other stars are likely to extract sufficient energy from the binary that a significant number will be detectable as coalescences observable today.

It was predicted (*et.al.*, 2010; Press and Teukolsdy, 1977) that such binaries are likely to be detectable at an even greater rate than neutron star coalescences. This prediction has been confirmed by the detection of a 30 solar mass binary black hole by Advanced LIGO. Because waveforms are very sensitive to the black hole spins and masses, (which depend on the formation mechanism), as more events are observed it will be possible to determine how the systems were formed, and in this way we will be able to derive information on the ancestors of the stars we see today in the modern universe.

1.3 Gravitational Wave Detection

Because gravitational waves are waves of gravitational tidal force, they apply a differential acceleration to a mass quadrupole (such as a long bar or a pair of separated test masses). Assuming a wave amplitude $h = \Delta L/L$, we can treat L as the effective spacing of the test masses or the length of the resonant bar. Thus the detection of gravitational waves becomes the task of measuring very small differential motions. In a solid bar a transient differential force can be detected as an acoustic excitation of the fundamental resonant mode. If freely suspended test masses are used, detection requires measurement of differential accelerations of the free masses.

Joseph Weber first considered the design of gravitational wave detectors in a book (Weber, 1961) and a paper published in 1960 (Weber, 1960). He considered

the gravitational wave energy absorbed by a resonant mass quadrupole such as a resonant bar. Recognising the significance of acoustic losses in increasing the effects of thermal noise, he proposed using large resonant masses in the form of disks or cylinders with very high acoustic quality factor. Transient bursts of gravitational waves with millisecond duration (as might be produced by the non-spherical birth of a black hole in a supernova or the final transient from a binary black hole coalescence) could cause excitation of modes with large quadrupole moment such as the fundamental longitudinal mode of a bar. He went on to construct two resonant bar detectors, one of which is shown in Fig. 1.2.

Fig. 1.2 Joseph Weber working on one of his aluminium bars.

Despite the smallness of the gravitational wave strain expected from likely sources, Weber undertook extended observations with a pair of resonant bars, using coincidence detection to distinguish between local noise sources (expected to be uncorrelated) and signals of cosmic origin, which would be correlated in both detectors.

In 1969, again in 1970, and in subsequent papers (Weber, 1970; Weber *et al.*, 1973), Weber published results claiming coincident excitation of his widely spaced pair of

detectors (one was located at the University of Maryland, the other was at Argonne National Laboratory). These observations were claimed to be the first detection of gravitational waves. The wave amplitude of individual bursts was estimated to be $h \sim 10^{-15}$. If valid, they would have represented a huge flux of gravitational waves corresponding to thousands of solar masses being turned into gravitational waves every year in the Milky Way, with each burst representing ~ 1 solar mass of gravitational energy being radiated isotropically.

Weber's claim had enormous repercussions which are still being felt today. Astronomers considered that the enormous flux and event rate implied by Weber's results to be impossible to reconcile with current astronomical knowledge. Many physicists were intrigued, and within a few years approximately 10 laboratories had built or were building Weber-type detectors. By 1972 results began to come in, which failed to confirm Weber's observations. There was anger and disillusionment amongst the physicists attracted to the field, but a small subset of the new groups were intent on building substantially improved detectors.

Weber's detectors used massive piezo-electric ceramics (commonly known as PZT) to read-out the vibrations of his resonant masses. Sensitivity was limited by electronics noise, and mechanical thermal noise partly due to PZT acoustic losses. By the Fluctuation-Dissipation Theorem, both acoustic and electrical dissipation directly translate to readout noise. Weber's bars represented one of the first examples in macroscopic experimental physics, where *back action* noise was manifested.

Back action noise was prominent because piezoelectrics are reciprocal devices. A displacement Δx creates a voltage ΔV and a voltage ΔV creates the same displacement Δx. Linear amplifiers such as operational amplifiers are always characterized by a pair of noise sources, normally described as current noise and voltage noise. Amplifier current noise leads to voltage fluctuations acting on the PZT, which create a noise force which acts directly back onto the mechanical system. This back action noise acting on the PZT applies forces to the mechanical resonator, which modifies its dynamical state. Because these fluctuations accumulate over time, their effects increase as the integration time is increased (corresponding to reduced measurement bandwidth). This behavior is opposite to that of voltage noise, which is simply additive, and *reduces* as the measurement bandwidth is reduced. The opposite bandwidth dependence of series noise and back action noise leads to a classical measurement limit similar to the now well known *standard quantum limit*. There is a minimum detectable energy that occurs at an optimum integration time. Increasing or decreasing the integration time (or its inverse, the measurement bandwidth) degrades performance.

In the early 1970's the standard quantum limit was unknown, but the noise analysis of resonant bars demonstrated a similar measurement limit in the classical regime. The standard quantum limit sets an energy detection limit set by the photon energy hf, for signal frequency f. The classical limit is $k_{\mathrm{B}}T_{\mathrm{n}}$, where T_{n} is the effective measurement *noise temperature*. In Weber's case the noise temperature was ~ 30K, or about $10^8 hf$. Optimum sensitivity occurred for a bandwidth of about 1Hz. Today back action noise is most familiar in optomechanics as radiation pressure noise.

Weber type bars at room temperature could only achieve a strain amplitude sensitivity $\sim 10^{-15}$. Cryogenic resonant bars that we will discuss below, exceeded the

sensitivity of Weber's bars by many orders of magnitude, and one of them, NIOBE, implemented the first high performance optomechanical type readout with microwaves. Laser interferometers went on to make enormous strides in optimizing optomechanical readouts. With these techniques detectors today have exceeded Weber's strain sensitivity by 6-7 orders of magnitude, corresponding to an astonishing 14 orders of magnitude improvement in gravitational wave flux sensitivity.

1.4 Cryogenic Bars and the First Parametric Transducers

Soon after Weber's first claims William Fairbank and Bill Hamilton proposed the use of cryogenic techniques to create resonant mass detectors of far greater sensitivity. Cryogenics would reduce thermal noise and allow the use of superconducting vibration transducers that in principle should allow extremely high sensitivity. Fairbank and Hamilton led groups at Stanford and Louisiana State University, with the initial goal of creating 5 tonne magnetically levitated resonant bars cooled to 3mK temperature. Hamilton proposed development of a radio frequency superconducting parametric transducer, while Fairbank proposed using a superconducting quantum interference device (SQUID) based transducer. The program was outlined in a paper published in 1974 (Boughn *et al.*, 1974).

In the above paper two superconducting transducer concepts were presented. One is the parametric transducer in which an acoustic signal modulates a resonant circuit, while the second involves direct modulation of supercurrents by a superconducting ground plane. The two concepts are illustrated in Fig. 1.3.

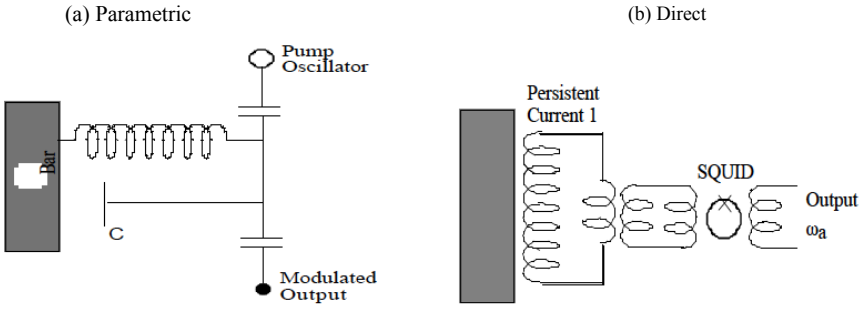

Fig. 1.3 Two concepts for high sensitivity transducers for gravitational wave detectors. The left side shows a parametric transducer in which motion modulates an LC circuit. The right side shows a superconducting circuit read out by a Superconducting Quantum Interference Device (SQUID) amplifier.

At Stanford Ho Jung Paik began development of a SQUID based transducer system based on superconducting flux conservation (Paik, 1976). Because magnetic flux LI (where L is inductance and I is current) is conserved in a superconducting circuit, and because the inductance of a flat pancake coil depends linearly on spacing to a superconducting ground plane, supercurrent is linearly modulated by proximity of a superconducting test mass in the form of a resonant diaphragm. Paik was the

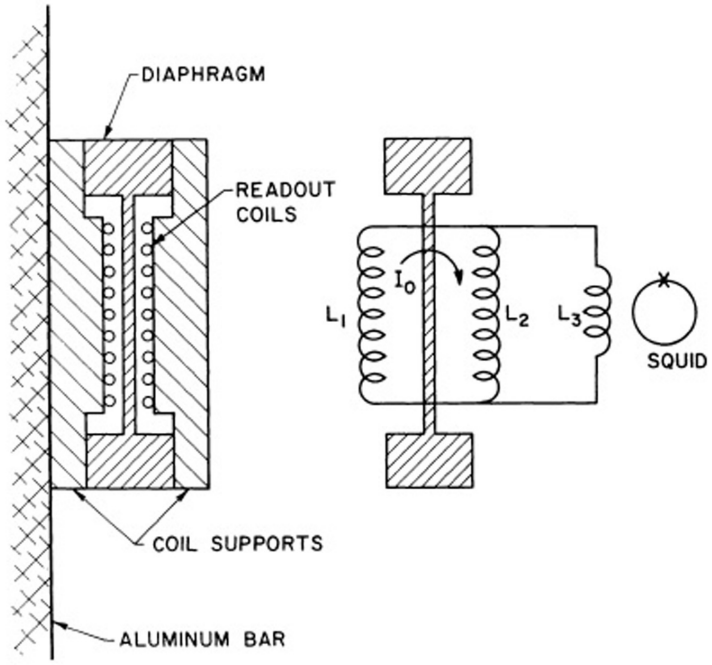

Fig. 1.4 The Paik transducer design. Motion of the diaphragm causes a difference current to flow through inductance L3 which is coupled to the SQUID.If the daphragm mode is tuned to the bar frequency this configuration embodies two mode impedance matching discussed later.

first to observe low acoustic losses $\sim 10^{-7}$ in annealed niobium at low temperatures, which was used both for the test masses and the inductive circuit. Like PZT, this inductive transducer was reciprocal, its forward transductance equal to its reverse transductance. However it obtained high sensitivity by using the extremely low noise of SQUID amplifiers and the low mechanical acoustic loss of the transducer. Figure 1.4 shows a schematic diagram of Paik's transducer.

At Louisiana State University Blair and Hamilton developed the first superconducting parametric transducer (Blair, Bermat and Hamilton, 1975). Like the Stanford transducer, the device made use of a superconducting pancake coil, but in this case it was used as part of a radio frequency LC-circuit, for which the frequency was modulated by the proximity of the surface of a superconducting test mass. The pancake coil was a thin film niobium-on-sapphire structure designed to achieve high radio frequency quality factor at 15 - 30MHz. This was the first gravitational wave transducer to make use of the non-reciprocal properties achievable through parametric upconversion. The acoustic signal frequency at $\sim$ 1kHz was up-converted to the radio frequency. The signal appears as a pair of signal sidebands, which must be demodulated to recover the acoustic signal. Due to the upconversion process the device is intrinsically non-reciprocal. As discussed in section 1.7, the forward to reverse transductance ratio is generally proportional to the frequency upconversion ratio.

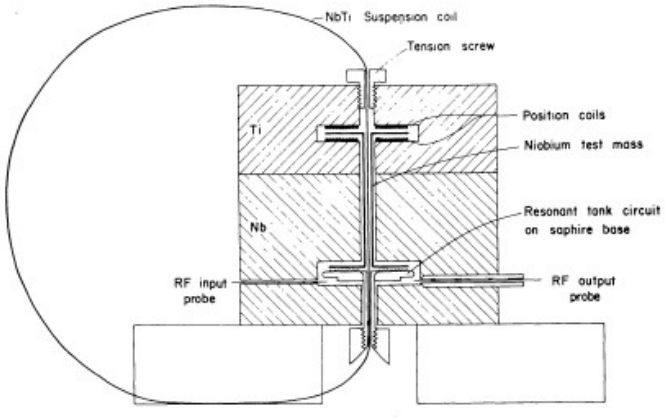

Fig. 1.5 Implementation of a magnetically levitated parametric transducer.Normal orientation was with the spindle axis horizontal. Coils at one end allowed the sensing surface to be located very close to a 12mm diameter niobium pancake coil etched on a sapphire substrate.

Figure 1.5 shows the design of this first parametric transducer. The device used a magnetically levitated niobium and sapphire spindle, with a sensing surface very close to the niobium-on-sapphire LC resonator. Magnetic levitation via a high supercurrent in a single loop of wire provided low acoustic loss. While this device achieved a sensitivity $\sim 10^{-17}$m/rtHz (Blair, 1979; Blair and Hamilton, 1979) detailed theoretical understanding of such devices was essential to their optimisation. This would only occur with development of microwave parametric devices described in the next section.

These first high performance superconducting transducers also exposed technical problems, which for the parametric transducer included the radio frequency power dependence of the superconducting LC circuit quality factor, and the need for an ultralow phase noise oscillator with which to excite the transducer.

Fairbank and Hamilton's proposal to build cryogenic gravitational wave detectors had ambitious goals. They aimed a) to reduce the temperature by a factor of 10^5 (300K to 3mK) so as to suppress the thermal noise energy, b) to increase the quality factor of the resonant bar by orders of magnitude to suppress the rate of thermal fluctuation, c) to use superconducting magnetic levitation to achieve exceptional vibration isolation, and d) to use superconducting transducers to achieve practically noise-free vibration measurements.They estimated that the signal to noise ratio could be increased by a factor of 10^6.

The above ambitious goals were realised to a large extent. While both technical and fundamental issues prevented the full benefits from being realised, the transducers provided a wealth of new physics and techniques that have had enormous impact on experimental physics ever since. Below we summarise the key issues and their outcomes.

Cryogenics and acoustic noise: The feasibility of cryogenic cooling of huge bars to

4K was quickly demonstrated, and groups in Italy led by Pizella and later Cerdonio successfully cooled 2300kg Al bars below 100mK.

Figure 1.6 shows a 2.3 tonne Al antenna,AURIGA, inside a cryostat which successfully cooled the bar to below 100mK using a dilution refrigerator. NIOBE achieved a quality factor greater than 10^8 at 5K.

However the benefits of cooling below $\sim$ 2K were never fully realised due to difficulties in cryogenic vibration isolation. Boiling liquid helium and gas flow in pipes is a significant acoustic noise source. Some detectors used cooling below the liquid helium superfluid transition at 2K to elliminate the noise of boiling helium. Others created much more elaborate vibration isolation systems that operated within the cryogenic environment. The best systems eliminated cryogenic noise by using very low pressure helium exchange gas as a thermal conductor with negligible acoustic transmission. However below 100mK the helium vapour pressure is too low to provide thermal conduction - gas effectively ceases to exist at this temperature. Thus at 100mK mechanical thermal links are required to extract heat and accomplish cooling. Such links also transmit vibrations.

Low acoustic loss systems: It was difficult to construct SQUID based transducer systems without acoustic losses associated with composite structures, so that very high quality factors were not observed except in the detector NIOBE (discussed in more detail below) which used niobium as the detector material, used low acoustic loss bonding, and contained minimal material with high acoustic losses.

Magnetic levitation: Magnetic levitation was only used successfully on small scale niobium prototypes (up to 67kg) because no methods were found for attaching high critical field superconducting material to a bar to enable magnetic levitation without unacceptable acoustic loss. Extensive studies in Western Australia demonstrated that the largest possible diameter for magnetic levitation of a niobium bar is about 200mm, limited by the critical magnetic field at which flux penetrates the superconductor.

Amplifier limits: SQUID amplifiers were expected to achieve quantum limited performance (see discussion below) but in practice noise performance was degraded when the SQUID was coupled to an external circuit.

Standard quantum limit: A major fundamental limitation that was completely overlooked in 1972 was that the proposed strain sensitivity brought detectors into the quantum regime. It came as a shock to the community that measurement of vibrations in highly macroscopic objects such as tonne-scale bars should be governed by quantum mechanics. In 1978 Braginsky et. al. (Braginsky, Vorontsov and Khalili, 1978) demonstrated the existence of the standard quantum limit, which followed much earlier work by Heffner (Heffner, 1962) on the quantum limit to linear amplifiers, later applied by Giffard (Giffard, 1976), to mechanical measurements with transducers. This recognition of the quantum nature of macroscopic measurements marked the beginning of the development of macroscopic quantum mechanics. In the next section we will discuss the first use non-contacting measurements with microwave re-entrant cavity parametric transducers.

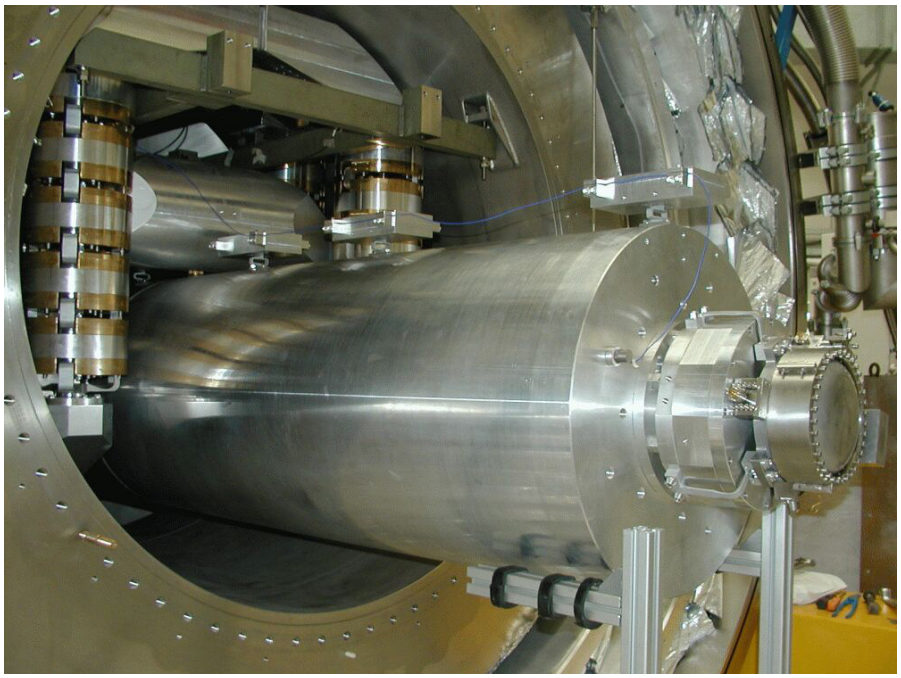

(a)

(b)

Fig. 1.6 a) The AURIGA aluminium bar that was cooled below 100mK and used a SQUID passive transducer, and b) the NIOBE detector, made from niobium, with a microwave parametric transducer.

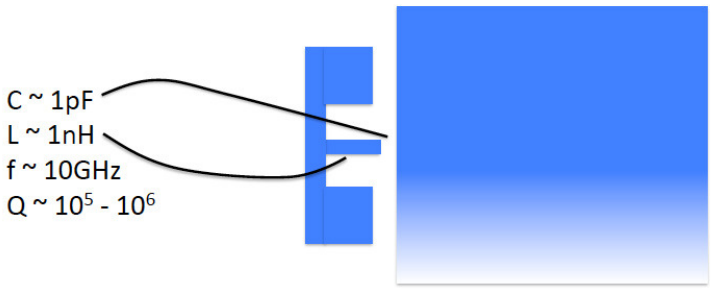

Fig. 1.7 A typical re-entrant cavity transducer (cross section) located near to the face of a cylindrical sensing surface, with a central post about 5mm long and 1mm diameter.

1.5 Non-contacting Superconducting Microwave Parametric Transducer

At Louisiana in 1974 Blair and Hamilton had demonstrated a Q-factor of 6×10^7 in a 6kg niobium bar. This led to the idea of building a large scale niobium detector which would combine low acoustic loss with the advantages of superconductivity. In 1975 a project began to develop a very high Q-factor niobium gravitational wave detector in Australia. Following a suggestion by Braginsky, and with much better understanding of the issues associated with parametric transducers, experiments began at UWA to explore the possibilities of using superconducting microwave parametric transducers based on re-entrant cavities, operating around 10GHz.

A re-entrant cavity is geometrically simple, rigid and robust, and if suspended about 50μm from a superconducting surface could achieve a high Q-factor $\sim 10^5 - 10^6$ with a very strong tuning coefficient $\sim$ 300MHz per micron due to capacitive modulation of the gap between the post (which is the main source of inductance) and the sensing surface. Figure 1.7 shows the cross section of a typical cylindrically symmetrical transducer configuration.

The re-entrant cavity made it possible to create a non-contacting transducer requiring no mechanical connection to the bar, thus helping to minimise the acoustic loss. Two sub-scale prototypes using a fully magnetically levitated bar combined with a similarly levitated transducer demonstrated the potential of this technology. However for a 1.5 tonne detector the transducer required a second mechanical impedance matching stage, and the diameter was too large for magnetic levitation. A non-contacting transducer system was still able to be implemented in slightly different form as discussed below.

Figure 1.8 shows two examples of a magnetically levitated re-entrant cavity transducer. Both cavity structures include choke sections in the form of a large ring groove which creates a large impedance mismatch for radially guided microwaves, so as to reduce radiation losses. A superconducting coil outside the choke section (in one case) creates a weak repulsive force between the transducer and the levitated bar. When levitated, with appropriate longitudinal magnetic springs, the transducer freely oscillates across resonance. A time trace of the demodulated signal output is shown in Fig. 1.9. It shows sharp transitions as the re-entrant cavity crosses resonance while oscillating

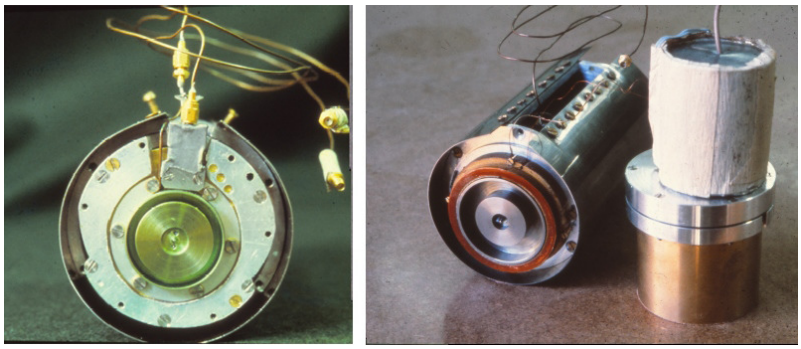

Fig. 1.8 Two different magnetically levitated re-entrant cavity parametric transducers.Left: a re-entrant cavity with narrow choke section. Right: Transducer with wider choke, superconducting repulsion coil also used for SQUID secondary sensing, and a superconducting frequency stabilisation cavity used to suppress phase noise.

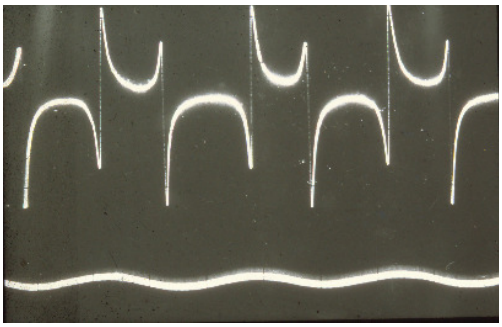

Fig. 1.9 Superconducting microwave parametric transducer response as it sweeps through the cavity resonance. The signal is derived from a double balanced mixer with the local oscillator phase adjusted to recover the phase shift across resonance. The sharp transitions represent the phase shift across resonance. This error signal was used to lock the cavity near the centre of resonance via forces applied through the voice coil. The bottom trace shows the sinusoidal motion of the transducer measured by the SQUID readout shown in Fig. 1.11.

at a frequency $\sim$ 10Hz with an amplitude of a few nm. A superconducting voice coil provided control forces to lock the transducer at the centre of resonance.

Figure 1.10 shows the levitation cradle for such a transducer, with a 50mm diameter niobium bar in its own levitation cradle. Levitation was achieved by pumping several hundred amps of persistent current into copper clad NbTi coils soldered to a stainless steel housing. The copper and the stainless steel provide resistive insulation for a zig-zag current loops that supports the levitated masses.

The system illustrated above was excited by a low noise klystron microwave source. It achieved a noise temperature $\sim 10^{-2}$K, three orders of magnitude better than a room temperature bar, but it also exposed limitations that would need to be solved for a large scale resonant bar.

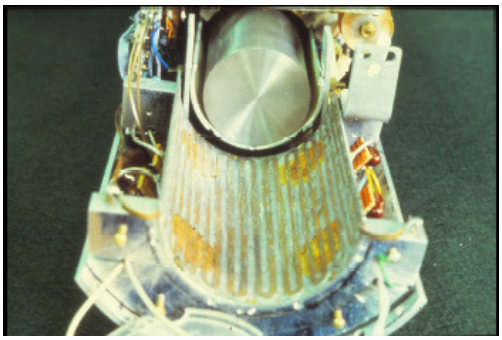

Fig. 1.10 Magnetic levitation cradles for a small Nb bar and a transducer. The bar diameter is 50mm. The transducer, supported by a NbTi alloy superconducting shield, is illustrated in Fig. 1.8. Bar and transducer were independently levitated. Radio frequency sense coils monitored the levitation height.

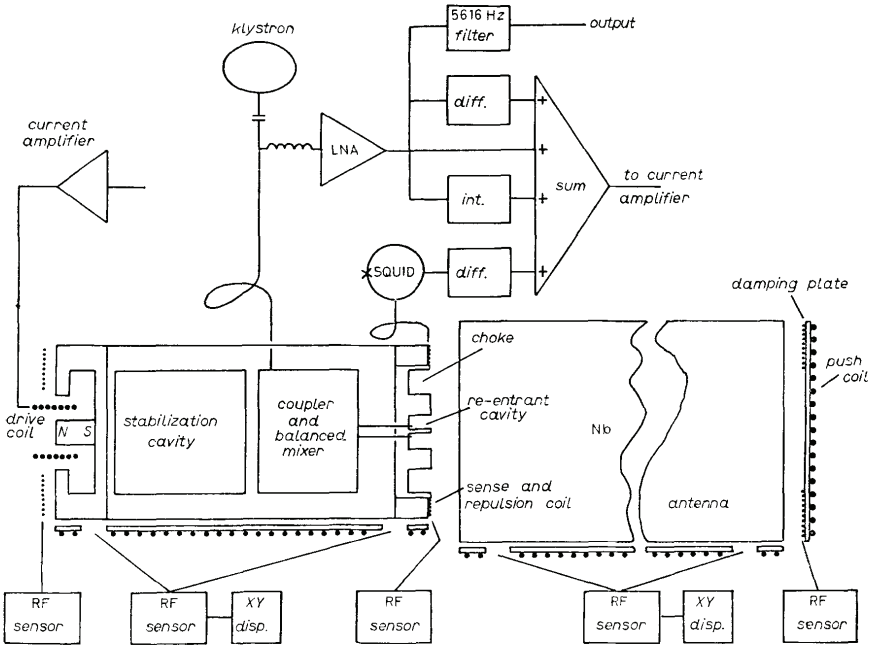

Fig. 1.11 Schematic diagram of the magnetically levitated gravitational wave detector described in the text above (Blair and Mann, 1981). The transducer required precision active control of the gap spacing since the position bandwidth of the re-entrant cavity was very small ($\sim 10^{-11}$ m) and low frequency motion at a few Hz was $\sim 10^{-4}$ m. A radio frequency sensor and a SQUID sensor provided hierarchical sensitivity for the gap spacing, for the purpose of control and calibration.

1.6 Coupling Coefficients, Thermal Noise and Effective Temperature

In the analysis of resonant bar antennas, the concept of the electromechanical energy coupling coefficient β was introduced to characterise the transducer. While in both types of transducer an acoustic signal in the resonant bar is converted into an electrical signal, the process is somewhat different for a direct transducer where the electromagnetic energy has the same frequency as the acoustic signal, and the parametric transducer, where the energy is transformed to modulation sidebands.

In a direct transducer with a capacitive sensor with capacitance C, it is straightforward to show that β is given by the ratio of the electrostatic energy divided by the mechanical energy of the mechanical resonator if its vibration amplitude x was equal to the capacitance gap. That is:

$$\beta_1 = \frac{\frac{1}{2}CV^2}{M\omega_{\mathrm{a}}^2 x^2}, \tag{1.3}$$

where ω_{a} is the resonant frequency of the bar antenna.

For the parametric transducer (Fig. 1.3) we obtain a similar expression, except that the coupling coefficient is increased by the frequency rati o between the mechanical freuqency of the bar and the pumping frequency ω_{p}.

$$\beta = \frac{\omega_{\mathrm{p}}}{\omega_{\mathrm{a}}} \frac{\frac{1}{2}CV^2}{M\omega_{\mathrm{a}}^2 x^2}. \tag{1.4}$$

This result implies that a large frequency ratio is advantageous. However, because a high resonant frequency generally requires a much smaller capacitor, the advantage occurs as long as the magnitude of the frequency ratio ($\sim 10^7$ for the transducers discussed here) exceeds the capacitance ratio (typically 10^3). Another factor in favour of the parametric transducer is that AC electric field breakdown threshold (which sets the maximum usable voltage across the capacitor) is usually substantially higher than DC breakdown. There are other important advantages of using parametric transducers as discussed further below.

It is important to understand why acoustic losses, or their inverse, the acoustic quality factor are so important in making low noise measurements of mechanical resonant devices. This is best explained in the context of a phase space description of the state of the oscillator. We are interested in the measurement of the fundamental mode of a resonant bar because as discussed above, it has the highest quadrupole moment and couples most strongly to gravitational waves. However the discussion is relevant measurements of any mechanical modes. We start with a simple but incomplete classical description of a resonant bar readout, shown in Fig. 1.12. The state of the resonant bar can be expressed in terms of amplitude and phase coordinates, but a much more elegant description uses phase space quadrature coordinates.

Figure 1.12 shows a bar coupled to a transducer with coupling coefficient β. After amplification, the transducer output is demodulated to zero frequency, using a reference oscillator at the bar frequency ω_{a}. This process gives rise to two quadrature values X_1 and X_2. A vector from the origin has magnitude equal to the resonator amplitude,

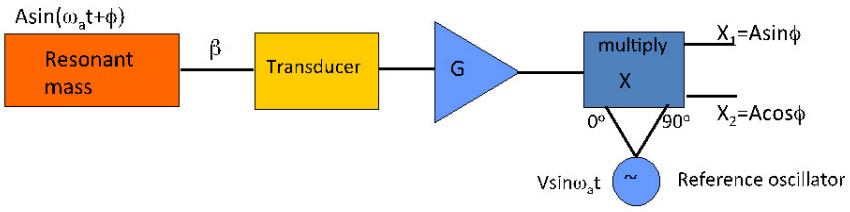

Fig. 1.12 A classical resonant mass coupled to a transducer, with an amplifier of gain G and demodulated to zero frequency to record the two quadratures $A\sin\phi$ and $A\cos\phi$. It is assumed that the transducer output signal is at the bar antenna frequency $\omega_{\rm a}$.

and phase angle corresponding to the phase difference between the reference oscillator and the acoustic mode.

This picture, shown in Fig.1.13, allows us to understand the role of acoustic losses in measurements of mechanical resonators. First suppose the Q-factor was infinite. Then the bar would be a perfect harmonic oscillator with constant amplitude and phase. In this case the phase space coordinate of the bar is a stationary point with fixed phase and amplitude.

In reality every mode is coupled to the thermal reservoir: the enormous set of acoustic modes that define the heat capacity of a material, and which contribute fluctuating forces that lead to mechanical thermal noise or Brownian motion. This coupling, which depends inversely on the Q-factor, causes the amplitude and phase of mechanical modes to fluctuate while maintaining a mean energy of $k_{\rm B}T$. In phase space, the state of the mode is no longer a fixed point. It undertakes a random walk. If the Q-factor is very high the velocity of the state vector random walk in phase space is very low. There is a clear and simple correlation: high Q = weak coupling to the thermal reservoir = slow motion in phase space.

Now suppose you want to measure an external force which acts on the resonator to change its state vector. If you make a measurement in a short period of time $\tau_{\rm m}$, compared with the mechanical relaxation time $\tau_{\rm a}$, the changes in the state vector will be small, so the thermal noise contribution will be minimised. However, if the measurement time $\tau_{\rm m}$ is long compared with $\tau_{\rm a}$, the noise energy will be comparable to $k_{\rm B}T$. In general if the measurement takes place in a short time $\tau_{\rm m} \ll \tau_{\rm a}$, the noise energy change will be reduced by the factor $\tau_{\rm m}/\tau_{\rm a}$. The phase space coordinates are illustrated in Fig.1.13. The vector $(P1, P2)$ represents the state change between two successive measurements. The magnitude of this vector will be reduced the higher the resonator Q-factor.

Referring to Fig. 1.12, let us ask about the role of the coupling factor β. The coupling factor scales the amount of mechanical resonator energy that appears in the transducer. It reduces the total phase space change. Because there is always additive noise (as we will discuss later), reduction in β causes the measurement time to be increased and the thermal noise contribution to increase. Thus small β = longer measurement time = reduced sensitivity.

Thus the sensitivity of many mechanical measurements depends on the factor

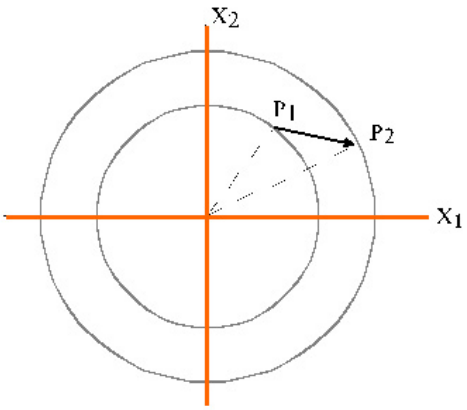

Fig. 1.13 Phase space coordinates and state vectors for successive measurements. The state vector for a high Q resonator undertakes a random walk due to thermal noise, but the length of the difference vector between pairs of measurements $(P1, P2)$ is reduced if the Q-factor is high.

β. Today many experiments aim to eliminate thermal noise in mechanical resonator measurements (Underwood *et al.*, 2015; Aasi, 2015). These typically need factors of $\beta Q \sim 10^{12}$.

The reduction of thermal noise in high Q resonators can be expressed by the concept of noise temperature: the magnitude of the energy fluctuations expressed in degrees Kelvin.

Weber's detectors achieved a noise temperature of about one tenth of the ambient temperature, $\sim$ 30K through use of high Q-factor. The NIOBE detector, discussed below, achieved a noise temperature $\sim 2 \times 10^{-4}$ of the 5K operating temperature (Blair *et al.*, 1995).

1.7 Impedance Formalism for Transducers

Using a single parameter β to characterise mechanical resonators coupled to transducers, as we considered above, is a gross over-simplification. We did not consider the additive noise from the amplifier, nor did we consider the fact that there is no such thing as a perfect one way valve. The last concept is behind the uncertainty principle, which appears in any careful analysis, whether classical or quantum.

From a classical standpoint all of the above is encapsulated in the impedance formalism. The concept of impedance is used extensively in radio frequency electronics and transmission lines (such as the 50Ω input impedance of many radio frequency devices). If impedances are matched at any junction, then there is maximal power flow without reflection. If there is an impedance mismatch, then energy is reflected at the interface.

However impedance is a much more general concept that can be applied to all forms of wave energy. A dielectric mirror is a device designed to offer a high impedance

mismatch for light, while an anti-reflection coating matches the impedance of free space to the impedance (for light) of a lens or window. A human ear contains complex structures to match the acoustic impedance of the sensing system to the acoustic impedance of the air. We will see that impedance matching was extremely important to the design of cryogenic gravitational wave bar detectors.

Transducers can be described in the following matrix formulation which links the force F and velocity u at the transducer input to the voltage V and current I at the output. Linking these quantities is the 2×2 impedance matrix $\mathbf{Z}$.

$$\begin{bmatrix} F \\ V \end{bmatrix} = \begin{bmatrix} Z_{11} & Z_{12} \\ Z_{21} & Z_{22} \end{bmatrix} \begin{bmatrix} u \\ I \end{bmatrix} \tag{1.5}$$

The four terms of $\mathbf{Z}$ can be determined for every transducer. A full 2-port description of the measurement chain then needs only to have included the effective noise properties of the amplifier to obtain a full theoretical description of system performance. Figure 1.14 shows this schematically. The amplifier has gain G and two noise terms, the voltage noise spectral density S_{e} and the current noise spectral density S_{i}. The transducer has a mechanical input impedance Z_{11}. This term has units of force per unit velocity, or $kg.s^{-1}$, and characterises the compliance of the transducer input. We will see that this term can be strongly tuned in parametric transducers, whether they be on resonant bars, optomechanical microresonators or laser interferometer gravitational wave detectors. The force and velocity are associated with the interaction between the bar and the transducer.

The second term in the 2-port matrix is the forward transductance Z_{21}, which has units of volts per meter per second, $Vm^{-1}s^{-1}$. This term describes the magnitude of the output voltage due to a mechanical input measured as a velocity.

The terms associated with the output are the output impedance Z_{22} and the reverse transductance Z_{12}. The latter term has units of $kg.amp^{-1}$. In general Z_{12} is always finite. It determines how the output circuit, in particular the current noise, is able to act back on the input such that a voltage fluctuation at the output creates a

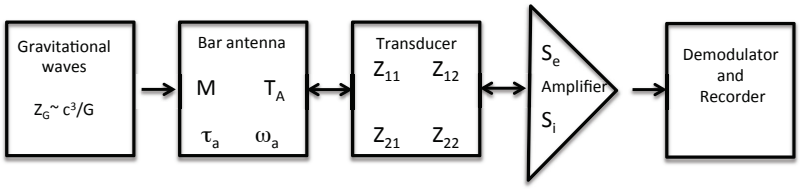

Fig. 1.14 A schematic diagram showing the measurement chain for a resonant mass gravitational wave detector. Gravitational waves with very high impedance as discussed in the text, interact with an antenna of mass M, temperature T_{A}, relaxation time τ_{a} and frequency ω_{a}. The transducer is described by four impedance matrix components, with force and velocity at the imput and voltage and current at the output. The transducer is amplified by a linear amplifier with voltage noise S_{e} and current noise S_{i}. Both ends of the chain are classical, where back action can be ignored, but in between back action plays an important role.

force fluctuation at the input. This force acts back on the mechanical resonator and behaves similarly to the fluctuating forces from thermal noise. It creates a noise term that increases as the measurement integration time increases, and is responsible for a classical uncertainty principle that limits the performance of any classical transduction system. The same physics is described in different language in optomechanical systems (see section 1.11.1). The reverse transduction in optomechanics often arises from quantum radiation pressure noise, or in the classical regime, the intensity noise of the laser light.

The output impedance Z_{22} of the transducer is a simple electrical quantity measured in ohms. The only requirement for this term is that it satisfies an electrical impedance matching condition with the amplifier.

In parametric transducers, which are intrinsically resonant devices, there is large flexibility in their pump frequency, from radio frequency to optical, their tuning, their Q-factors and their linewidths. The transduction matrix contains Lorentzian terms associated with their resonant circuits which can provide strong resonant amplification or suppression of signal sidebands. We will see later that this flexibility allows surprising properties such as electromagnetic or optical springs (the name depends on the nature of the pump radiation), self cooling, and negative dispersion.

To explore the properties of parametric transducers it is often useful to use mixed pictures, sometimes thinking about them from a quantum picture, and sometimes from a classical circuit standpoint. In the next section we will review the quantum picture.

1.8 The Quantum Picture For Parametric Transducers

In section 1.3 we looked at the general structure of a parametric transducer, while in section 1.7 we examined a general 2-port matrix formulation for transducers. Now we will restrict our analysis to parametric transducers, noting their most important characteristic: they scatter radiation from a pump oscillator into modulation sidebands. Conventionally parametric transducers create a pair of modulation sidebands. The pump oscillator at frequency ω_p is modulated by the mechanical resonator at frequency ω_a. The modulation sidebands occur at frequency $\omega_\mathrm{p} \pm \omega_\mathrm{a}$. However single sideband devices can also exist. One example is the three mode opto-acoustic parametric amplifier (Zhao *et al.*, 2009) which we will discuss in section 1.12.

If we consider parametric transducers from a quantum mechanical viewpoint we must consider the mechanical resonator to be a system of phonons and the pump oscillator to provide a stream of photons. In this picture the transducer scatters photons with phonons as illustrated in Fig. 1.15. In the quantum picture there are two separate processes taking place simultaneously. They can be described by simple vertex diagrams as shown in Fig. 1.16.

Both Figs. 1.15 and 1.16 emphasise one key point. If energy is conserved in quantum scattering, and if the pump oscillator is a source of photons entering the transducer, then the signal phonon power flow direction is uniquely determined by the sideband frequency. The upper sideband can only be created if a phonon from the mechanical resonator add to the energy of the pump photons. Therefore acoustic energy must flow out of the resonator to create an upper sideband. Similarly a lower sideband photon

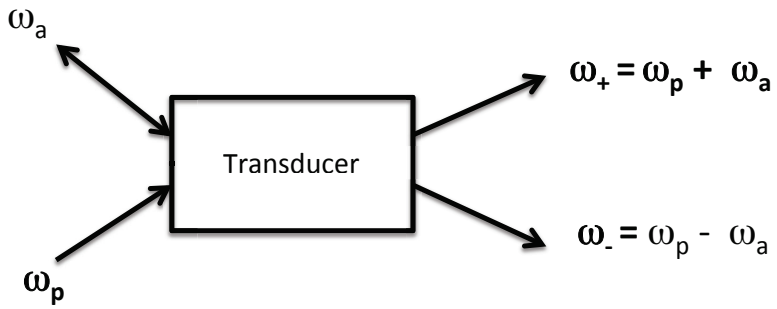

Fig. 1.15 Diagram of a transducer as a device that scatters mechanical resonator phonons ω_{a} with pump photons ω_{p}, to create photons at the upper and lower sideband frequencies $\omega_{\pm}$.

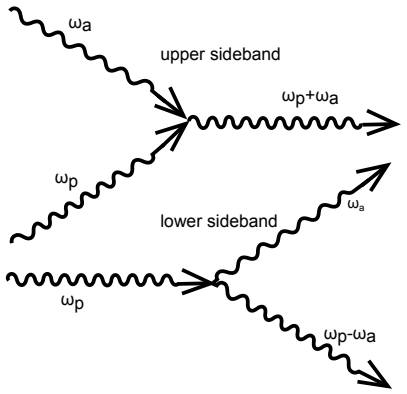

Fig. 1.16 The processes illustrated in Fig. 1.15 have been broken down into two separate scattering processes, one which creates upper sidebands and the other which creates lower sidebands. Notice that the power flow direction for the phonons has opposite directions.

can only be created if phonon energy ω_{a} is extracted from ω_{p}. This phonon energy must flow back into the resonator.

The above ideas were proved classically by Manley and Rowe for lossless nonlinear electrical circuits in the 1950s (Manley and Rowe, 1956). Both the classical and quantum approaches are direct results of energy conservation, but in the quantum picture the conclusions are quite obvious as we saw above.

We have to add just one additional observation to come to a very important conclusion. We started by considering the parametric transducer as a high Q electrical circuit pumped at its resonance. However the pump frequency does not need to match the transducer electrical resonance. If the transducer cavity frequency (such as the re-entrant cavities discussed earlier) is tuned so that its resonance matches the lower

sideband frequency, then naturally the lower sideband will be preferred over the upper sideband. This condition is called blue detuning because the pump oscillator frequency is above the cavity frequency. From a classical standpoint, the lower sideband will have an enhanced amplitude, but from a quantum standpoint excess phonons will flow into the mechanical resonator, increasing its occupation number.

Equally if the cavity is tuned so that its resonance matches the upper sideband frequency, (a red detuned pump oscillator) then more phonons will flow out of the mechanical resonator. Its phonon occupation number will decrease.

These changes in occupation number are described as heating or cooling of the mode. Mode cooling, also called self damping or cold damping, reduces the quality factor of mechanical modes, but in a noiseless way, without addition of classical noise. Hence the term cold damping. Mode heating starts by increasing the mechanical resonator Q-factor (but not in a way that increases thermal noise), but at higher pump power levels can lead to instability when the phonon injection rate exceeds the loss rate from the intrinsic quality factor of the mechanical resonator. This is called parametric instability.

Cold damping can be very useful. High Q systems are very difficult to work with because accidental excitations may go on ringing endlessly and can often exceed the measurement system dynamic range. Apply cold damping and there is no change in noise performance (because the thermal reservoir is still providing the same fluctuating force) but the modes damp rapidly and the equilibrium signal amplitude is low.

In the above discussion we have ignored zero point motion. In 1962 Heffner (Heffner, 1962) showed that the uncertainty principle limits the noise temperature of a linear amplifier to

$$T_{\mathrm{n\_min}} = \frac{\hbar\omega}{k_{\mathrm{B}} \ln 2}. \tag{1.6}$$

This means that a transducer will always experience an additive noise contribution due to the amplifier which follows it, with a minimum possible added noise energy which according to Heffner is ~ 1.4 times the photon energy. Given the quantum limit to the noise energy, the amplifier must always have finite current noise. This acts back on the transducer via the reverse transductance Z_{12}. Thus a perfect linear transducer must always include back action noise which acts to disturb the mechanical resonator, and series noise which creates an additive contribution. Even for a lossless, transducer with zero classical noise, quantum noise and the thermal noise of the resonator itself sets significant limits to measurement.

In section 1.6 we saw that the effective temperature due to thermal fluctuations reduces as the ratio of the measurement time to antenna relaxation time $\tau_{\mathrm{m}}/\tau_{\mathrm{a}}$. The measurement noise (expressed as noise temperature T_{e}) is given by (Blair, 1980)

$$T_{\mathrm{e}} = \frac{2\tau_{\mathrm{m}}}{\tau_{\mathrm{a}}} T_{\mathrm{a}} + \frac{2\hbar}{k_{\mathrm{B}} \ln 2}, \tag{1.7}$$

where T_{a} is the temperature of the resonant bar antenna.

Remembering that $\tau_{\mathrm{a}} = Q/\omega_{\mathrm{a}}$, we can now specify the Q-value Q_{Q} required to reach the quantum limit given in Eq. 1.6. It follows that

$$Q_{\mathrm{Q}} = \frac{k_{\mathrm{B}} T_{\mathrm{a}} \tau_{\mathrm{m}}}{2\hbar}. \tag{1.8}$$

Similarly we can ask what temperature T_Q is required to achieve the quantum limit for a given Q-factor:

$$T_{\mathrm{Q}} = \frac{2\hbar Q}{k_{\mathrm{B}} \tau_{\mathrm{a}}}. \tag{1.9}$$

Any mechanical measurement using a transducer and linear amplifier must satisfy the above conditions to achieve quantum limited performance. For resonant bars, detector noise contributions include acoustic noise generated within the cryostats, non-ideal amplifiers and other noise sources. The best cryogenic resonant bar detectors came within 3 orders of magnitude of the quantum limit. In laser interferometer detectors where the physics of the measurement system is similar, detectors are within an order of magnitude of quantum limited performance and small scale optomechanical devices have achieved quantum limited performance at higher mechanical frequencies.

The above limits set by the Q-factor, temperature and quantum noise are valid for resonant mass gravitational wave detectors, and any resonator-transducer system where it is desired to detect external transient forces in which changes in the state of the resonator are measured in a time τ_{a} short compared to the mechanical relaxation time τ_{a}.

1.9 The impedance matrix for parametric transducers

By treating a parametric transducer as a quantum scattering device we have seen that there are two separate scattering processes, one which extracts energy from a mechanical resonator, and the other one that returns energy to the resonator. While the two port model discussed above is valid, it is useful to extend the formalism by treating the sidebands separately. This leads to a new impedance matrix in which we separate all the impedances into upper and lower sideband components, corresponding to the two diagrams in Fig. 1.16. The new impedance matrix, which identifies upper and lower sideband components by $+/-$ subscripts is given as follows

$$\begin{bmatrix} V_-(\omega) \\ F_1(\omega) \\ V_+(\omega) \end{bmatrix} = \begin{bmatrix} Z_{--} & Z_{-1} & 0 \\ Z_{1-} & Z_{11} & Z_{1+} \\ 0 & Z_{+1} & Z_{++} \end{bmatrix} \begin{bmatrix} I_- \\ u_1 \\ I_+ \end{bmatrix} \tag{1.10}$$

Here F_1 and u_1 are the force and velocity at the transducer input while $V_\pm$ and $I_\pm$ are the upper and lower sidebands voltage and current at the output.

In the impedance matrix, we see forward transductance components $Z_{\pm 1}$, which describe the signal transduction to each sideband. Similarly each sideband can independently act back on the input via $Z_{1\pm}$. Each sideband has a separate output impedance $Z_{--/++}$. However the input impedance does not separately access the sidebands, so this is given by Z_{11}. Here we summarise an analysis of parametric transducers presented by Blair (Blair, 1980), based on this approach. The analysis was based on the equivalent circuit shown in Fig.1.17.

The LC circuit in in Fig.1.17 assumes a parametric transducer with capacitive sensing, driven by a pump oscillator with frequency ω_p close to the LC resonance

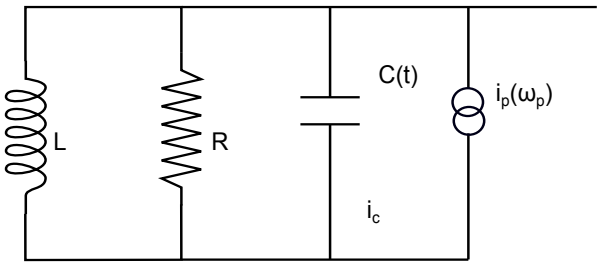

Fig. 1.17 Equivalent circuit for a parametric transducer. $i_{\rm p}(\omega_{\rm p})$ represents the pump oscillator.

frequency ω_0. Normally we are interested in low loss transducers for which R is small. Tuning of the pump frequency relative to the cavity frequency changes the magnitude and phase of the impedance components, and has particularly strong effects in the high electrical Q-factor limit, which is often described as the resolved sideband limit. In particular the input impedance and the forward transductance are very strongly tuned by the tuning of the pump frequency. Of particular interest is the extreme tunability of the mechanical input impedance.

The mechanical input impedance is given by the sum of two complex terms, one for each sideband, as given below.

$$Z_{11} = -\frac{\frac{1}{2}C_0V_{\rm p}^2}{\omega_{\rm a}\omega_0 x^2}\left[\frac{\omega_+ Q(1-2j\Delta_+ Q)}{1+4Q^2\Delta_+^2} - \frac{\omega_- Q(1+2j\Delta_- Q)}{1+4Q^2\Delta_-^2}\right], \tag{1.11}$$

where C_0 is the rms value of the capacitance of the transducer, $V_{\rm p}$ is the pumping voltage amplitude, Q is the quality factor of the transducer, $\omega_{\rm a}$ is the resonant frequency of the bar antenna and ω_0 is the resonant frequency of the cavity. In this equation the delta terms that describe the frequency detuning are given by

$$\Delta_\pm = \frac{1}{2}\left[\frac{\omega_\pm}{\omega_0} - \frac{\omega_0}{\omega_\pm}\right]. \tag{1.12}$$

Equation 1.11 can be re-written in terms of absolute detuning of pumping microwave field with respect to the cavity resoance δ, coupling coeffcient β, and the cavity damping rate γ defined as $\gamma = \omega_0/Q$. As we can see later, this rewrote formula is directly map to the input mechanical impedance of laser interferometer detectors Eq. 1.22, given by:

$$\begin{aligned} Z_{11} &= -j\frac{C_0V_{\rm p}^2}{\omega_0 x^2}\frac{\omega_p}{\omega_a}\frac{\delta}{(j\gamma/2+\delta-\omega_a)(-j\gamma/2+\delta+\omega_a)}, \\ &= -2j\frac{\beta\delta}{(j\gamma/2+\delta-\omega_a)(-j\gamma/2+\delta+\omega_a)}, \quad j=\sqrt{-1} \end{aligned} \tag{1.13}$$

where the second equality comes from the definition of coupling coefficient β in Eq. 1.4.

If the Q-factor rises high enough that the linewidth is small compared to the mechanical modulation frequency, the input impedance experiences a strong peak when the transducer is pumped at the sideband frequency.

While this resolved sideband behaviour was discovered in the context of resonant bar gravitational wave detectors described in the next section, it was not applied in this context because the electrical Q-factors were not high enough. However the same physics is relevant to laser interferometer gravitational wave detectors and to optomechanical devices.

The real part of the input impedance is shown in Fig.1.18 as a function of the detuning frequency $\delta\omega_{\rm p} = \omega_{\rm p} - \omega_0$. The real component is analogous to a resistive load in a transmission line. However in the parametric transducer it can be varied between large negative and positive values, and can be tuned to zero for small negative detuning. The same curve for positive detuning, on a log-log scale is plotted in Fig.1.19.

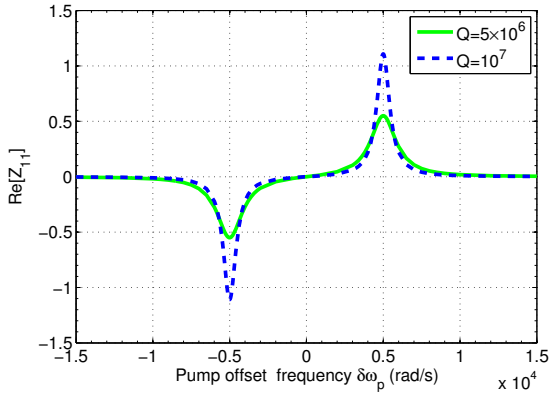

Fig. 1.18 The real part of Z_{11} for two values of quality factor showing the impedance changing between negative and positive values and near zero for zero detuning.

Remembering that an impedance ratio at an interface determines the transmitted and reflected power, negative input impedance describes a system for which the reflected mechanical signal power is greater than the incident mechanical driving power. Microwave parametric amplifiers created in the 1960's exploited similar negative resistance in varactor diodes to enable reflective amplification of microwaves. In the context of transducers, negative impedance can lead to instability. However in the context of laser interferometers, mirror acoustic mode amplification by three mode interactions (a form of resolved sideband parametric transducer) have been shown to be useful as a means of predicting parametric instability at higher power (Ju *et al.*, 2014).

Large positive mechanical input impedance describes a situation where the mechanical input impedance can be tuned to match the mechanical output impedance of a mechanical resonator, under which conditions the transmission of acoustic power is optimised. In the case of the NIOBE gravitational wave detector, a parametric transducer was matched to a secondary coupled mechanical resonator attached to the resonant bar, as discussed in the next section. The third interesting case, zero input impedance, describes the case where the transducer has minimal interaction with the mechanical signal source. It draws no net energy from the mechanical resonator.

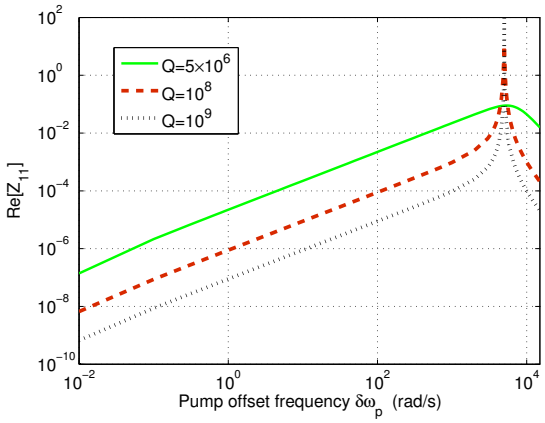

Fig. 1.19 The real part of Z_{11}, shown with log scales. We see that high Q-factor suppresses the detuned input impedance except for when the detuning matches the sideband frequency. The sideband frequency used here was chosen to match the frequency of the NIOBE detector.

In 2015 Ma and Blair *et al* applied an analysis similar to the impedance analysis above, to a laser interferometer gravitational wave detector (Ma *et al.*, 2015*a*), to answer the question: do laser interferometers absorb energy from gravitational wave detectors? While the analysis was presented in a modern quantum framework, its derivation was equivalent to the 1979 results discussed here. Laser interferometers today operate with near zero detuning and hence near zero mechanical input impedance. As the above analysis shows, the impedance can be raised by using detuning, such that the energy absorbed from gravitational waves is maximised.

This important result replaces the resonant bar with spacetime itself. The impedance mismatch of interest is that between spacetime and the suspended mirrors of a laser interferometer. The laser interferometer is a parametric transducer, which has tunable input impedance. If the input impedance is raised, more of the gravitational wave signal will be absorbed by the interferometer. Intuitively one would expect that this could increase the signal to noise ratio but this conjecture has not yet been proved.

The imaginary part of the input impedance is also very important. This is like a reactance in a transmission line and for the transducer it represents electromagnetic stiffness, which in opto-mechanics is described as an optical spring.

In general the reactive component of the input impedance can strongly tune the resonant frequency of the mechanical resonator, while the resistive components tune the damping. The slope of the reactance curve determines whether the spring constant is positive or negative, while the magnitude of the real part determines the damping.

If the negative spring of the transducer exceeds the positive spring of the mechanical resonator it can create dynamical instability similar to that of an inverted pendulum.

Fig.1.20 shows the reactive component of the input impedance for two values of quality factor. The slope of these curves determine the strength and the sign of the optical spring. For zero detuning the spring term is zero but for detuning equal to the sideband frequencies strong positive and negative springs appear. A very important

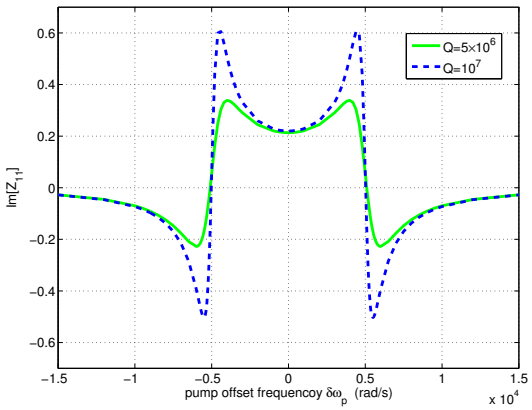

Fig. 1.20 The imaginary components of the input impedance represent the "optical" spring properties of parametric transducers which create positive or negative damping and cause the transducer to change the mechanical frequency of the resonator as shown experimentally in Figs. 1.27 and 1.28.

property of the springs is apparent from comparison of the above curves: positive springs are associated with negative damping, while positive damping is associated with negative springs.

In the next section we will see results from the resonant bar NIOBE that confirmed the above behaviour. Interestingly, the strength of the electromagnetic spring was sufficient that a few milliwatts of microwave power could significantly tune the resonant frequency of a 1.5 tonne mechanical resonator.

We now go on to discuss the forward transductance of the parametric transducer. The two sideband components (indicated by the + and - signs) of the forward transductance are given by:

$$Z_{\pm 1} = \pm \frac{V_{\mathrm{p}} Q}{2x\omega_0} \left(\frac{\omega_{\mathrm{p}}}{\omega_{\mathrm{a}}} \pm 1 \right) \left(\frac{1 - 2j\Delta_{\pm} Q}{1 + 4Q^2 \Delta_{\pm}^2} \right). \tag{1.14}$$

Normally both sidebands of the transducer will be amplified and demodulated together. Then it is appropriate to combine both sideband transductances into the combined forward transductance which is equivalent to the term Z_{21} of Eq. 1.5. Then the total signal voltage for double sideband detection V_{DSB} is given by

$$V_{\mathrm{DSB}} = (|Z_{+1}| + |Z_{-1}|) u_1. \tag{1.15}$$

As a function of detuning the forward transductance shows a resonant peak at the sideband frequencies, especially for high Q-factor. However Fig. 1.21 shows also that the transductance is only weakly dependent on detuning for small detuning. This means that a transducer in which there is say, weak seismic noise modulation causing the gap spacing to be modulated, will have negligible changes in transductance if the modulations are small compared with the sideband frequency. However, such motion

would be accompanied by significant input impedance variations as shown in Figs. 1.19 and 1.20.

This phenomenon of impedance variation due to the offset frequency dependence of optical springs is very important in ground based gravitational wave detectors. Low frequency seismic-induced motions are difficult to avoid. They always give rise to seismic frequency modulation. The phenomenon was clearly observed in the NIOBE detector and is commonly observed in laser interferometer detectors. In NIOBE low frequency tracking was used to minimise this effect.

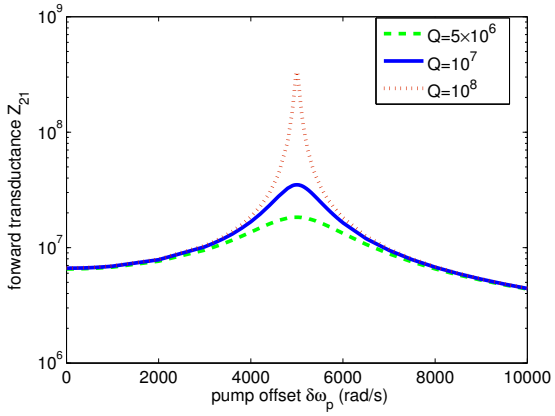

Fig. 1.21 The forward transductance is not strongly dependent on detuning except in the high Q-limit, where it can be substantially enhanced.

1.10 The design of NIOBE, a 1.5 tonne resonant bar with superconducting parametric transducer

In the previous sections we have seen the implementation of non-contacting re-entrant cavity transducers controlled in three dimensions and vibration isolated by magnetic levitation. The impedance formalism for parametric transducers was presented, and results were used to illustrate the complex behaviour of such systems.

The need for impedance matching has been emphasised in the preceding sections. Matching to a lower impedance increases the mechanical amplitude and decreases the applied force. This acts to increase the signal to noise ratio if the transducer performance is dominated by series noise, such as the noise generated by frequency fluctuations of the pump oscillator.

The output impedance of a mechanical resonator such as a large bar is given by $M\omega_a$. Its large magnitude is difficult to match to a small transducer. The mechanical input impedance is determined by the transducer parameters as discussed above, and is tunable by changing the magnitude of the pump signal. To obtain reasonably good impedance matching for NIOBE a secondary resonator mass of $\sim$ 1kg was desirable.

The simplest means of impedance matching is to couple a low mass harmonic oscillator to the high mass oscillator. This provides narrow band impedance matching,

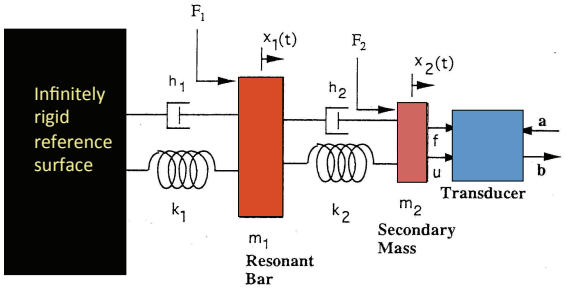

Fig. 1.22 Mechanical model of a 2-mode antenna with a transducer. Such models can easily be extended to multi-element impedance matching stages. In general impedance matching allows increase in bandwidth.

because the coupled harmonic oscillator transfers energy between the resonator components on a relatively long time scale. Broadband impedance matching was exquisitely developed in the days of the acoustic gramophone. Devices such as levers and acoustic horns were used to couple the high impedance of a stylus needle moving in a record groove, to a the low impedance of the air. Devices based on tapered whip-like cantilevers also allow broadband resonant gain. If several tuned mass harmonic oscillators are connected in a chain with successively lower masses it is possible to achieve N-stages of impedance matching. Figure 1.22 shows a block diagram of a two stage system, which can easily be elaborated to include additional stages (Blair *et al.*, 1987).

Figure 1.23 shows the predicted bandwidth of various single, two and three stage impedance matching networks. In the presence of significant noise sources, both sensitivity and bandwidth are increased by using extra stages. Yet these curves also emphasise the intrinsic narrow band nature of resonant bar detectors, compared with laser interferometers that achieve $\sim$ 1kHz bandwidth.

The concept for the readout of NIOBE was chosen to facilitate a) impedance matching; b) a means for a simple low acoustic loss mechanical design for the re-entrant cavity transducer; and c) a non-contacting coupling as illustrated in Figure 1.24. The need for simple mechanical integrity was emphasised because complex mechanical elements such as nuts and bolts have always been well known as sources of acoustic loss.

A simple single impedance matching element consisting of a pure niobium tapered bending flap on a massive base was used (Fig. 1.24). It was attached to the bar using very thin layers of epoxy resin bonding pads to create a very low loss acoustic bond. It was this innovation that allowed the antenna to be operated without input and output cables. Instead a pair of microstrip antennas enabled radiative coupling of the microwave signal into and out of the transducer. This eliminated a critical source of noise: acoustic vibration from the noisy cryogenic environment transmitted as transverse acoustic waves through flexible cables.

The transducer shown in Fig. 1.24 had a single short semi-rigid cable between the transducer and the microstrip antenna. It was fixed in location to prevent induced vibration and losses. A simplified diagram is shown in Figure 1.25.

To obtain optimum noise performance a cryogenic microwave high electron mobility transistor (HEMT) amplifier with noise temperature just a few times larger than the

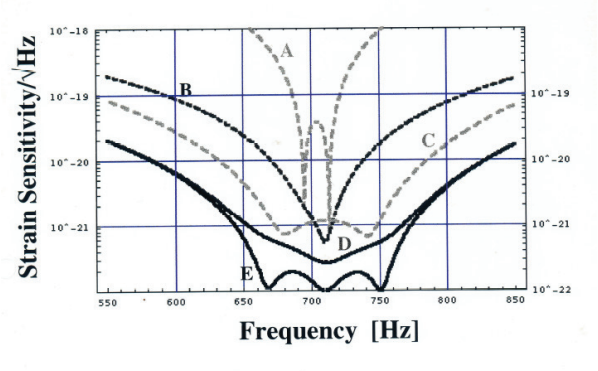

Fig. 1.23 Strain sensitivity curves showing the possibility of improving both bandwidth and sensitivity of resonant mass gravitational wave detectors by modified impedance matching. Curve A shows the sensitivity of NIOBE. Curve E shows the ultimate achievable sensitivity that could have been achieved using three mechanical modes for improved impedance matching combined with a quantum limited amplifier and reduced oscillator phase noise. Possible intermediate cases are also shown.

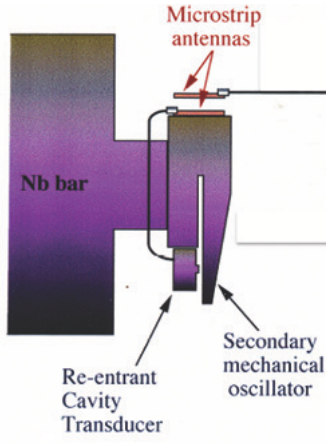

Fig. 1.24 Schematic diagram of the NIOBE transducer system showing the re-entrant cavity parametric transducer and the non-contacting readout system. The base side of the transducer was thicker than shown here to prevent epoxy-induced distortions from deforming the gap spacing during cooldown. Figure 1.22 shows a mechanical model of the secondary resonator.

quantum limit ($T_{\mathrm{n}} \sim 6\mathrm{K}$) was chosen to amplify the signal from the re-entrant cavity. Such amplifiers, designed for radio astronomy, have excellent noise performance but only if the signal level is very small.

While the expected signal sidebands from the vibration amplitude of the niobium bar would be small, it would normally be almost impossible to set the microwave couplings at each interface to be so close to unity that a significant amplitude of

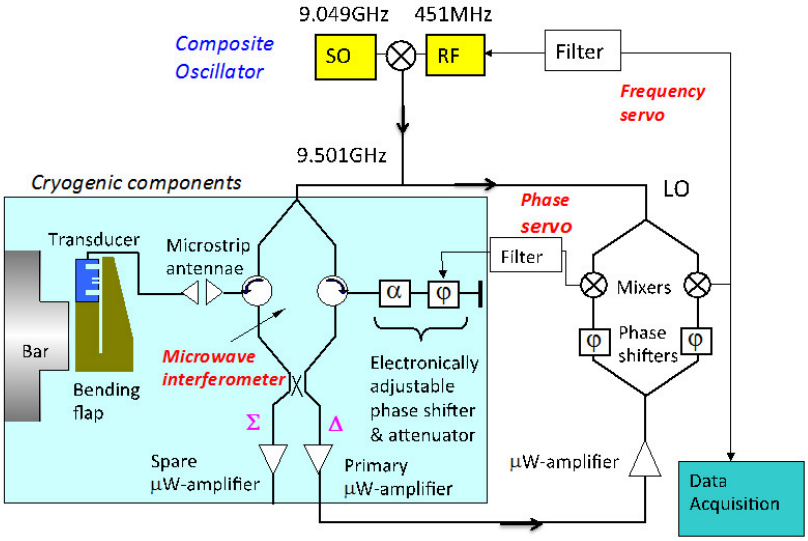

Fig. 1.25 The readout system for NIOBE which included a cryogenic interferometer and a sapphire loaded cavity oscillator (SO) and a non-contacting readout system to prevent cryostat acoustic noise from reaching the bar, and a servo system for compensating for phase changes.

carrier signal would not be reflected back into the amplifier.

To overcome the consequent amplifier saturation problem, a cryogenic interferometer was used to suppress the microwave carrier signal. The signal was obtained at the differential "dark port" of the interferometer. This allowed the HEMT microwave amplifier signal level to be maintained at less than about -60dBm. Electronically adjustable phase shifters and attenuators were required to provide the correct amplitude and phase of pump signal such that the the pump power at the amplifier was sufficiently suppressed.

The phase shifters and attenuators themselves had to be specially developed for the NIOBE transducer. They consisted of high permeability low loss ferrite-loaded stripline circuits for which the permeability could be tuned using a superconducting solenoid. Tuned beyond their transmission line cut-off, the devices acted at attenuators, while in the linear regime they acted as phase shifters. Three such devices in series were required to access 2π phase shift and up to 20dB attenuation. They operated with fixed trapped supercurrents. A fourth device was used to provide a small servo controlled phase correction signal to compensate for low frequency changes in the spacing across the non-contacting antennas due to residual pendulum motion of the niobium bar (Ivanov *et al.*, 1993). This was required because the bar, suspended by a long chain of vibration isolation components, acted like a simple pendulum with a rocking frequency below 1Hz.

An unavoidable problem was caused by having the re-entrant cavity fixed in location relative to the sensing surface of the bending flap, rather than being magnetically levitated in the configurations discussed earlier. Because the microwave resonant frequency of the transducer could not be adjusted, it was impossible for this frequency to be matched to the frequency of a fixed frequency low phase noise oscillator. Precision bonding of the cavity to the transducer assembly to about 0.3 microns resolution caused 100MHz errors in the transducer frequency.

As part of the NIOBE project ultralow phase noise sapphire loaded cavity oscillators had been created, with quality factors $\sim 10^{10}$. These oscillators had exceptionally low noise, but could not be tuned to the transducer frequency (Tobar and Blair, 1992). A variable frequency low phase noise source was required as the pump oscillator.

When oscillator signals are mixed to create a new frequency, the noise performance is generally dominated by the worst oscillator. The best option at that time was to choose a frequency in the frequency band where the best possible frequency synthesisers could be used in conjunction with an ultralow phase noise oscillator of fixed frequency. The composite oscillator so created consisted of a sapphire loaded cavity oscillator (Tobar and Blair, 1992), combined with the best Hewlett-Packard frequency synthesiser operating at around 450MHz.

The entire microwave assembly shown in Figure 1.25 combined very high performance cryogenic microwave electronics consisting of the supercurrent tuned phase shifters, attenuators, circulators and microwave amplifiers, operating in a vacuum at 5K. The room temperature demodulation section included two mixers for deriving the main signal output and the servo control signal used to compensate for the low frequency rocking of the suspended niobium bar. The entire systenm work remarkably well over many years. Thanks to masterful microwave and electronic engineering by Eugene Ivanov, the phase servo worked so well that only in very large earthquakes, when rocking amplitudes rose to $\sim$ 5mm, did the servo control systems lose lock.

One of the first experimental problems encountered when working with very high Q-factor mechanical resonators is that they can be excited accidentally and maintain very large amplitudes for many hours as shown in Fig. 1.26. This makes experiments difficult and can lead to saturation of amplifiers and consequent excess noise. A simple solution to this problem is the use of self damping or mode cooling through red-detuning of the pump oscillator to the 3dB point of the transducer cavity response. Self damping of the 1.5 tonne Nb bar was very effective. The Q-factor of mechanical modes at 694Hz and 713Hz were reduced by 3 orders of magnitude using a few hundred microwatts of incident microwave power as shown in Fig. 1.27. In Fig. 1.28 full data for the electromagnetic spring effect in NIOBE is shown. Because it takes some time for parametric instability to build up it was possible to explore the electromagnetic springs in the blue detuning regime where the Q-factor becomes infinite.

NIOBE operated for long periods of time between 1993 and 2000 in the 5-detector International Gravitational Events Collaboration. Four of the detectors used SQUID transducers. NIOBE alone used a parametric transducer. The detector array was able to set new upper bounds on the strength and the rate of gravitational wave bursts (Allen *et al.*, 2000). First experimental search for gravitational wave bursts was conducted by a network of resonator bar detectors, at a sensitivity $\sim 4 \times 10^{-21}/\sqrt{\text{Hz}}$.

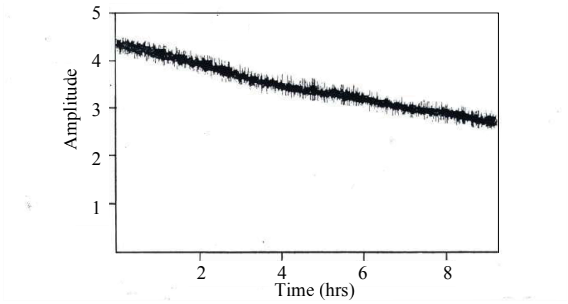

Fig. 1.26 A ringdown curve for NIOBE, showing amplitude decay of the 700Hz fundamental mode by about 25% in six hours.

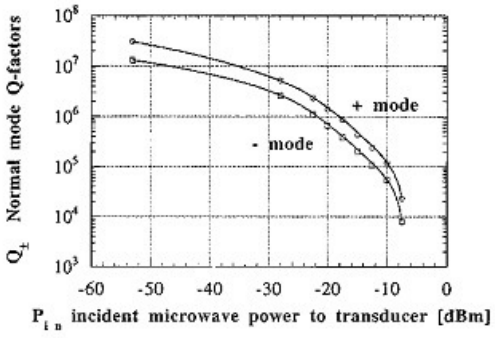

Fig. 1.27 Self cooling as a function of microwave pump power. The Q-factor of the fundamental acoustic modes of the 1500kg Nb bar-transducer system was reduced by a factor 10^3 using a few hundred microwatts of input power.

During the development of NIOBE the UWA group was also exploring other transducer technologies. Of particular interest here is the sapphire dielectric transducer (Peng, Blair and Ivanov, 1994; Cuthbertson, Tobar, Ivanov and Blair, 1998). The transducer element consisted of a pair of whispering gallery mode sapphire dielectric resonators structured as a face to face pair of mushrooms. They operated at microwave frequencies. The transducer was tuned by the interaction of the evanescent waves between the resonators. This transducer had a high Q-factor at room temperature $\sim 10^6$ K, and could be expected to have an extremely high Q-factor at cryogenic temperatures $Q \sim 10^9$. While its tuning coefficient was lower than that of a re-entrant cavity, this was outweighed by its high Q-factor. The entire device is shown in Fig.1.29. It used an interferometric readout in which one arm contained a reference sapphire loaded cavity resonator. In the cryogenic regime the device operated in the resolved sideband limit for audio frequency signals. A room temperature version was tested on a Virgo superattenuator, and yielded very impressive sensitivty, able to see low fre-

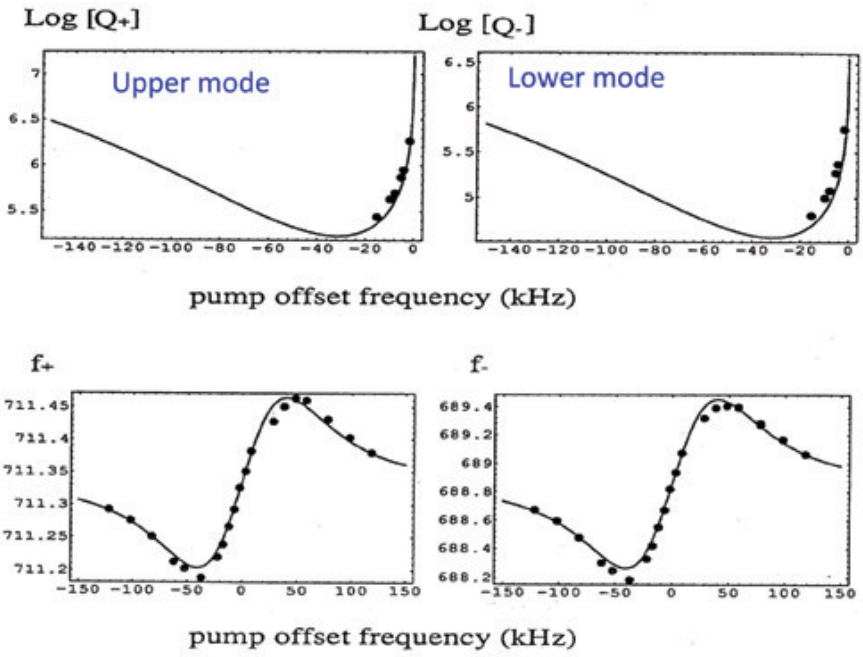

Fig. 1.28 The frequency dependence of the real and imaginary parts of the input impedance act on the two longitudinal normal modes of NIOBE to change both the quality factor (top curves) and the mode frequency (bottom curves). Red detuning lowers both the quality factor and the mode temperature (i.e.the thermally excited amplitude distribution) because it enhances the coupling to the upper sideband which absorbs energy from the resonator. Detuning also creates an electromagnetic spring through the imaginary components of the input impedance. A few hundred microwatts of microwave power is sufficient to cause one mode of the 1500kg bar to be detuned by more than 1Hz.

quency acoustic modes that were hidden by the noise of conventional accelerometers, as shown in Fig.1.30 (Peng and Blair, 1994).

While gravitational waves were not detected by resonant bar detectors, they set important upper limits. NIOBE uncovered the beautiful physics of optomechanics with parametric transducers, and was able to make displacement measurements $\sim 10^{-19}$m. The best noise temperature of about 100μK was achieved in the final run in 2000. Of particular significance, NIOBE contributed understanding and knowhow which could be applied to laser interferometer gravitational wave detectors, from high performance vibration isolation to the fundamental optomechanics of the devices themselves.

1.11 Advanced Laser Interferometer Gravitational Wave Detectors

In previous sections, we have seen the conceptual similarity between the designs of resonant bar detectors with parametric transducer and the laser interferometers. Many important design ideas of modern laser interferometric gravitational wave detectors, such as interferometric readout for balancing the technical noises, resonant cavities,

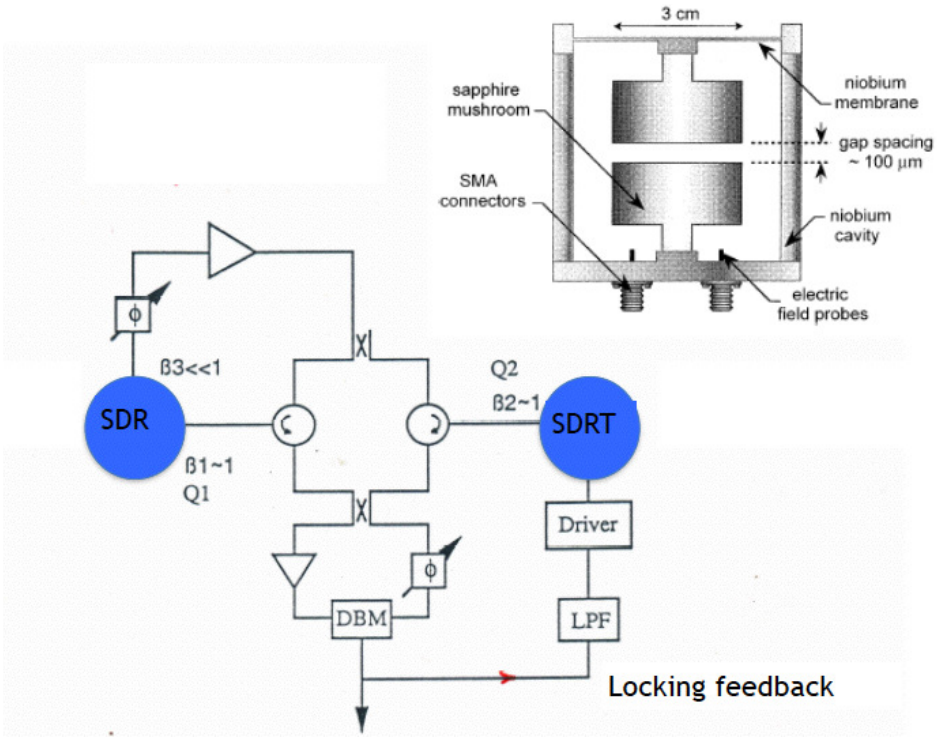

Fig. 1.29 The sapphire dielectric cavity transducer. High Q-factor whispering gallery modes interact through their evanescent fields. A solid spindle sapphire loaded cavity configured as a loop oscillator provides a microwave field and acts as pump oscillator for the interferometric pair of resonators. The solid resonator has high Q and low phase noise while the split resonator is sensitive to acceleration due to its membrane suspension. The transducer resonator is locked to the microwave source via a very low frequency feedback loop which applies a weak force to the membrane.

frequency stabilisation, etc, can be found in the design of readout system of the NIOBE resonant bar detector. Moreover, many of the important physical principles in modern laser interferometric detectors such as the quantum limit, and modification of the system dynamics by optomechanical interactions were manifest in the physics of bars with parametric transducers. This similarity is not surprising. Both the principles of interferometric detectors and the parametric transducer readout of a resonant bar are based on the coupling between mechanical degrees of freedom and electromagnetic fields. Both are optomechanical parametric transducers.

The differences between the bar detectors and the interferometric detectors are also important to highlight, because they deepen our conceptual understanding of both systems. First, as we saw earlier, the bar detector used the extremely high-Q acoustic vibration of the bar to suppress thermal noise. This led to a relatively narrow detection bandwidth. Laser interferometers also use high-Q resonance to suppress thermal noise.

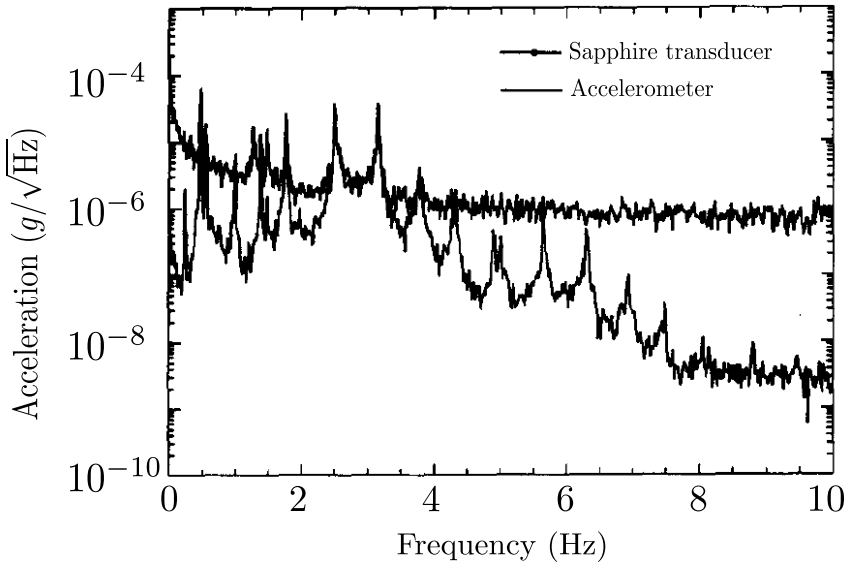

Fig. 1.30 The calibrated acceleration responses of a sapphire parametric transducer compared with a high quality accelerometer. Both devices were suspended on the bottom of a high performance multistage "superattenuator" vibration isolator developed for the Virgo laser interferometer gravitational wave detector. Numerous acoustic modes in the 0-10Hz band were only discernable with the sapphire transducer accelerometer.

However by measuring the spacing between nearly free masses, the laser interferometer achieves relatively large detection bandwidth especially if it works in the so-called resonant sideband extraction mode as used by Advanced LIGO.

In the resonant bar, the gravitational wave tidal forces do work on the bar, thereby exciting the fundamental internal longitudinal acoustic mode of the resonant bar. In interferometers the center of mass of the mirrors respond like test particles to the incoming gravitational tidal forces. At the technical level, the electromagnetic fields used for sensing the motion of test masses is at the optical frequency in laser interferometers, where as we saw above, microwave fields were used for NIOBE. This "simple" change of electromagnetic wave frequency makes a big difference for detector sensitivity, since advanced optical coating technology allows the creation of ultra-high optical power (several hundred kWs). In late 1990s, the interferometer designs finally won the race for sensitivity.

On 14 September 2015, Advanced laser interferometers (AdvLIGO) detected the gravitational waves from a black hole binary coalescence event (Abbott, 2016). This

detection was a great triumph of optomechanics. Advanced laser interferometers are very sophisticated parametric transducers that directly receive gravitational wave signals. The improvement of LIGO by a factor ~ 3 in strain sensitivity (compared with initial LIGO in 2006) brought signals over an audibility threshold. Below threshold we could not resolve signals. Above the threshold we could recognize signals and obtain a remarkable amount of information regarding black holes that were probably created by the first massive stars in the universe. The discovery confirmed the theory of detection in which laser beams measure spatial strains between freely suspended test masses. It also gave us a calibration for astrophysical signals which allows firm predictions of the benefits of sensitivity improvements. It opened the era of gravitational wave astronomy.

Now that signals have been detected, the payoff in increasing LIGO sensitivity is enormous. Each factor of 3 improvement increases the accessible volume of the universe by approximately $3^3 = 27$ times. This has multiple benefits: a) It increases the event rate for the type of sources already detected ($\sim 30 - 30$ solar mass black holes) by 27 times allowing statistical studies to begin. b) It greatly increases the signal to noise ratio of nearer events (such as those already detected) allowing much greater resolution of system parameters and deeper testing of general relativity, and c) it increases the probability of detecting new sources such as stochastic backgrounds and continuous wave sources.

The first detection of gravitational waves combined the optomechanics of kilometer-scale high optical power dual recycling interferometers, with the minimization of thermal noise by use of very high Q-factor mirrors and suspensions, and prevention of unwanted optomechanical three-mode interactions that lead to instability. In this section we will focus on specific aspects of interferometric detectors a) their fundamental nature as parametric transducers, b) the parametric interactions that can cause instability, and c) the use of optomechanics to create devices able to enhance the sensitivity of gravitational wave detectors.

1.11.1 Laser interferometer as a parametric transducer

The schematic diagram of Advanced LIGO is shown in Fig.1.31. In essence the device measures changes in distance between two widely spaced mirrors, through the phase shift of a very high quality factor optical mode, due to cavity length changes. The cavity quality factor is approximately the cavity finesse (set by the mirror reflectivity and transmissivity) times the number of free space wavelengths in the cavity. Typically the quality factor is 10^{12}.

In practice single cavity detection is not currently possible, due to technical noise sources. A Michelson interferometer configuration allows the detector to become a differential device like a Wheatstone bridge, in which technical noise sources such as intensity and frequency noise are balanced out. The microwave interferometer in the NIOBE transducer readout (Fig.1.25) played a similar role. The 4km arm cavities in the interferometer are designed to enhance the signal by multi-reflections. Theses two arms are carefully matched so that the laser field will destructively interfere at the dark port (See Fig.1.31). Under the influence of gravitational waves one cavity

is lengthened when the other cavity is shortened and the beamsplitter extracts this signal at the dark port.

A real detector contains a succession of serial and nested optical cavities with optical linewidths varying from Hz to MHz. While complex, we want to emphasise that fundamentally the detectors are parametric transducers similar to the transducers we discussed earlier. Similar to the bar detector, the basic structure of laser interferometer can be described by the general block diagram we saw earlier (Fig.1.14) for a resonant bar with a parametric transducer. Instead of using a resonant bar as an intermediary device between the gravitational waves and the transducer, the antenna and transducer are integrated into a single device. The test mass mirrors and the Fabry-Perot Michelson interferometer form the parametric transducer. The pump frequency is the stabilised laser light which is detected by homodyne detection at the beamsplitter.

In the local Lorentz frame, the optomechanical interaction between the cavity field and the test mass differential motion transduces the mechanical signal to the optical signal by phase modulation of the optical cavity laser field. As with the other parametric transducers we considered, strong optomechanical coupling is required to obtain a large transduced signal.

The method for increasing the optomechanical interaction is to enhance the intracavity laser field intensity by adding a power recycling mirror (PRM). Because the interferometer operates with a dark fringe at the output, the laser input power is normally reflected. The power recycling mirror resonates the pump laser light within the interferometer, allowing substantial power build up as long as the technical power losses from scattering and absorption are low. The invention of power recycling was a breakthrough that allows the creation of very high optical power interferometers without the need of extremely powerful laser sources. For example, in current running AdvLIGO, a 20W laser source can create $\sim$ 150kW intra-cavity power, enhanced by a factor of 7500. This power recycling concept was invented by Ron Drever at a Les Houches Summer School in 1981 (Drever *et al.*, 1981). While increasing the optomechanical coupling, the high power also suppresses quantum shot noise.

The power recycling interferometer can be treated as a simple Fabry-Perot interferometer with a much higher power laser. In the presence of gravitational waves of frequency Ω, the intracavity laser field is perturbed by relative test mass motion at this frequency. This perturbation generates two signal sidebands with frequencies $\omega_0 \pm \Omega$. The signal is extracted at the dark port of the interferometer.

The gravitational wave signal frequency Ω appears only at the dark port of the interferometer, because of the asymmetric action of the gravitational waves. Common path effects in the two arms are canceled at the interferometer dark port. It is therefore possible to resonantly enhance the signal sideabands at the dark port by introducing a signal recycling mirror (SRM) (Meers, 1988). The signal recycling mirror sees a composite cavity created by the two input test mass mirrors.

The design of advanced laser interferometer detectors combines power recycling and signal recycling, and is normally described as a dual recycling interferometer. This dual recycling interferometer can be described using two effective single cavities as shown in Fig.1.31 (For details, see (Buonanno and Chen, 2003)).

Earlier we saw how the behaviour of parametric transducers could be modified

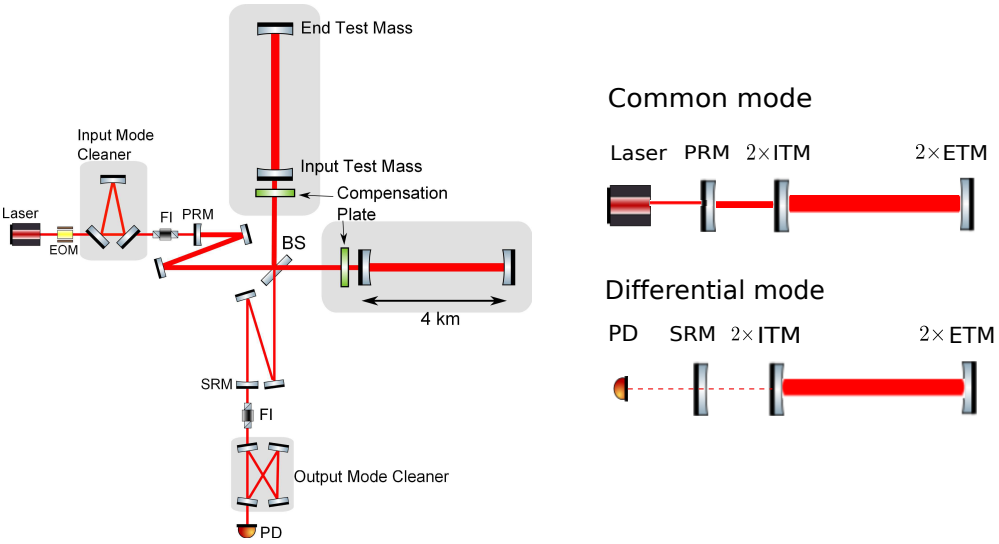

Fig. 1.31 A simplified schematic diagram of Advanced LIGO showing the main optical cavities. Left panel: the Dual Recycling interferometer configuration. This configuration can be described by two effective single-cavities as shown in the right panel. The common mode cavity corresponds to equal length changes in both arms. The differential mode cavity is sensitive only to differential length changes between the two arms, such as those created by gravitational waves. The common mode cavity is normally chosen to be resonant with the pump laser frequency for maximal build-up of intra-cavity power. The resonant frequency of differential mode cavity is detuned by tuning the signal recycling mirror. Since the common and differential modes both involve motion in the two interferometer arms, these equivalent representations require the mass of test mass mirrors and the intra-cavity power to be doubled compared to a real detector. (Buonanno and Chen, 2003).

by detuning the pump frequency relative to the cavity resonance frequency. In a very similar manner, many new possibilities are introduced to laser interferometer detectors by tuning the signal recycling cavity. For example, the tuning of the position of the signal recycling mirror changes the phase of the equivalent mirror created by signal recycling mirror and input test mass mirror. For this reason, adjusting the position of signal recycling mirror is equivalent to the detuning of the parametric transducer in Section 1.9, which leads to optomechanical changes to the dynamics of the differential motion of the test masses, through the action of optical springs.

For parametric transducers we used a 3×3 impedance matrix to describe the relationship between the input and output quantities as given in Eq.1.10. Here we use a similar formalism to describe laser interferometers. Specifically we need to be able to describe how the intra-cavity laser field is disturbed by noise sources, such as the quantum fluctuations that enter from the dark port, stochastic motion of the test mass mirrors driven by thermal fluctuations and seismic motion and classical optical noise due to light scattering and other processes. These disturbances contribute noise that contaminate the signal field. Here, for simplicity, we only consider the quantum noise

entering the dark port of the interferometer and develop an impedance matrix similar to Eq. 1.10.

Impedance measures how a physical system responds to external excitation: mechanical impedance describes the velocity response to the external forces; electronic impedance describes the voltage generated by the injected current. In optical resonator systems, the impedance tells us how the cavity responds to inputs, which may be mechanical motion or optical fields. The impedance matrix formalism presented here is not normally used. However, the individual input-intracavity field relations are widely used in computing the sensitivity of gravitational wave detectors, for example see Ref. (Kimble *et al.*, 2001).

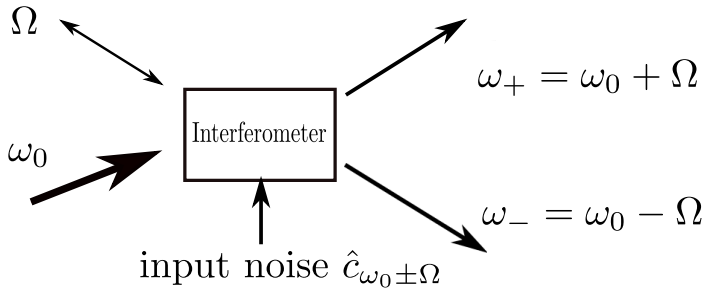

Fig. 1.32 Transducer diagram of interferometer systems. The thick arrow here is the pumping laser field with frequency ω_0. It is modulated by the test mass motion driven by gravitational waves at frequency Ω. The input quantum vacuum also enters the system and contributes quantum noise.

The impedance matrix we present below in Eq. 1.16 actually relates the input fields and the relative velocity of the test masses to the intra-cavity fields of the interferometer and the force acting on the test masses. For comparison, we used the same impedance subscripts as in Eq. 1.10. This new impedance matrix, together with a simple equation (Eq. 1.17) that relates the intra-cavity fields to the outgoing fields, provides a useful tool for analyzing the quantum behavior of the laser interferometer.

In Eq. 1.16 we denote the sideband frequency component of the input vacuum fields that enters the dark port of the interferometer by $\hat{a}^{(\dagger)}_{\omega_0\pm\Omega}$[1]. These fields can also be modified by squeezing.

The intra-cavity sideband fields, denoted by $\hat{A}^{\dagger}_{\omega_0\pm\Omega}$, are connected to the input fields by the output impedance Z_{++} and Z_{--}. The intra-cavity fields are also connected to the test mass velocity v_Ω by the forward transductances Z_{+1} and Z_{-1}.

Unlike the previous impedance matrix Eq. 1.10 which is based on a simplified classical model given in Fig.1.17, here we have non-zero impedance matrix elements Z_{+-} and Z_{-+} which connect the upper and lower sideband fields. These terms arise because radiation pressure creates correlations between the sidebands, described as pondermotive squeezing.

[1] $\hat{a}$ and $\hat{a}^{\dagger}$ are the annihilation and creation operator of light quanta

The force acting on the test mass F_Ω is connected to the input vacuum fluctuation fields by the reverse transductance terms $Z_{1\pm}$. This term, as before, describes back action or radiation pressure noise. The connection between the force acting on the test masses, and their relative velocity is given by the detector input impedance Z_{11}.[2]

All the above relations are summarised in the 3×3 impedance matrix given below:

$$\begin{pmatrix} \hat{A}_{\omega_0+\Omega} \\ F_\Omega \\ \hat{A}^\dagger_{\omega_0-\Omega} \end{pmatrix} = \begin{pmatrix} Z_{++} & Z_{+1} & Z_{+-} \\ Z_{1+} & Z_{11} & Z_{1-} \\ Z_{-+} & Z_{-1} & Z_{--} \end{pmatrix} \begin{pmatrix} \hat{a}_{\omega_0+\Omega} \\ v_\Omega \\ \hat{a}^\dagger_{\omega_0-\Omega} \end{pmatrix}. \tag{1.16}$$

The connection between the intra-cavity field and the output field is given by:

$$\hat{b}_{\omega_0\pm\Omega} = -\hat{a}_{\omega_0\pm\Omega} + \sqrt{2\gamma}\hat{A}_{\omega_0\pm\Omega}, \tag{1.17}$$

where γ is the bandwidth of the optical resonance peak of the interferometer differential mode, which is determined by the parameters of input test masses, end test masses and the signal recycling mirror.

Now we will present the formula of the individual impedance matrix elements in detail. First, the matrix elements Z_{++} and Z_{--} with dimension $[\mathrm{Hz}]^{-1/2}$ can be written as:

$$Z_{++/--}(\Omega) = \pm j\sqrt{\frac{\gamma}{2}}\frac{\alpha + 2\Omega^2(\mp j\gamma + \delta \mp \Omega)}{\Omega^2[\delta^2 + (\gamma - j\Omega)^2] - \alpha\delta}. \tag{1.18}$$

Combined with Eq. 1.17 which connects the intra-cavity fields to the output fields, Z_{++} and Z_{--} can be effectively considered as output impedance. Here $\alpha = 8\omega_0 I_c/mLc$ represents the optomechanical interaction strength, where $\omega_0, I_c, m, L, c, j$ are the pumping laser frequency, intra-cavity power strength, mirror mass, cavity length, speed of light, and $\sqrt{-1}$ respectively. The optical detuning δ is the frequency difference between optical resonance peak of the interferometer differential mode and the pumping laser frequency ω_0), determined by the parameters of signal recycling cavity.

Second, the forward transductances Z_{+1} and Z_{-1} with dimensions $[m^{-1}\mathrm{Hz}^{-1}]$ are given by

$$Z_{\pm1}(\Omega) = \frac{j(\sqrt{\alpha}/L)[\pm(\Omega + j\gamma) - \delta]}{\Omega^2[\delta^2 + (\gamma - j\Omega)^2] - \alpha\delta}. \tag{1.19}$$

They describe the signal transduction to each intra-cavity sideband field. Because photon number is dimensionless, the transductance quantities are slightly different from the voltage and current transductances of the classical formalism.

In the quantum regime, the input fields $a_{\omega_0\pm\Omega}$ are the fluctuating quantum light entering into the cavity. This means that the force generated through reverse transductances Z_{1+} and Z_{1-} acts back on the test mass motion. This is the back-action noise that comes from the radiation pressure force fluctuations, similar to the back-action

[2]Note that here we use Ω to represent the mechanical frequency, different from the notation ω_a used in the discussion of bar detectors

noise due to fluctuation currents in the previous transducer formalism Eq. 1.10. The reverse transductance Z_{1+} and Z_{1-} has dimension $[\mathrm{N}\cdot\mathrm{Hz}^{-1/2}]$ and is given by:

$$Z_{1\pm}(\Omega) = \frac{\sqrt{\hbar m\gamma\alpha}}{2}\frac{1}{\gamma - j(\Omega \pm \delta)}. \tag{1.20}$$

The most interesting optomechanical physics manifest themselves in the matrix elements Z_{-+} and Z_{+-}, and in the mechanical input impedance Z_{11}. As mentioned above, the former describes pondermotive squeezing while the input impedance describes optical spring effects. The optomechanical interaction mixes the upper and lower sideband fields through impedance matrix elements Z_{-+} and Z_{+-}:

$$Z_{-+/+-}(\Omega) = \mp\frac{j\alpha\sqrt{\gamma/2}}{\Omega^2[\delta^2 + (\gamma - j\Omega)^2] - \alpha\delta}. \tag{1.21}$$

Note that these terms vanish when we turn off the optomechanical interaction ($\alpha = 0$). This pondermotive mixing establishes a correlation between the phase and amplitude fluctuations of the vacuum light, resulting in the generation of a squeezed light. The squeezing angle and degree of squeezing are determined by the optomechanical coupling strength. The physical process of this correlation is that the radiation pressure force noise which characterized by the optical amplitude fluctuation drives the motion of test mass, then enters into the phase of the optical field (Kimble *et al.*, 2001) through phase modulation.

Pondermotive squeezing is one of the most important characteristics of optomechanical systems. This squeezing effect exists even for basic optomechanical systems, such as a light beam interacting with a reflective mirror without any cavity structure. Pondermotive squeezing was first observed by (Purdy *et al.*, 2013). It could lead to a new sources of squeezed light as long as the mechanical resonator is not corrupted by thermal noise (Corbitt *et al.*, 2006; Purdy *et al.*, 2013).

The second important characteristic of optomechanical systems, as we saw on NIOBE, is their optical springs. This arises, as we saw earlier, from optomechanical modification of the input mechanical impedance Z_{11} with dimension $[\mathrm{N}\cdot\mathrm{s}\cdot\mathrm{m}^{-1}]$, represented by:

$$Z_{11}(\Omega) = jmL\Omega - \frac{jm\alpha}{4\Omega L^2}\frac{\delta}{(\Omega - \delta + j\gamma)(\Omega + \delta + j\gamma)}. \tag{1.22}$$

Here the first term represents the mechanical impedance of the tess mass system. This term does not appear in Eq 1.11 beacause in the case of the resonant bar this mechanical impedance is the impedance to which we are trying to match. For the interferometer the gravitational wave is the signal sources, that sees both the mechanical impedance of the test masses and the additional impedance due to the transducer. It is clear that the second term of Eq.1.22 has the same form as Eq. 1.13, which shows the unity of the physics of the microwave-bar system and the laser-mirror system. In detuned laser interferometers, the optical spring can actually enhance the sensitivity in a narrowband way since the response of test mass is increased when the gravitational wave frequency is close to the optical spring frequency.

Current Advanced LIGO is built based on a non-detuned configuration with $\delta = 0$. Therefore the test mass dynamics is not modified and the previous impedance matrix elements can be greatly simplified, making the physics behind these formulae more transparent. For example, in the non-detuned case the transductance Z_{++} and Z_{--} can be written as:

$$Z^{\delta=0}_{++/--}(\Omega) = \frac{\sqrt{2\gamma}}{\gamma - j\Omega} \pm \frac{j\alpha\sqrt{\gamma/2}}{\Omega^2(\gamma - j\Omega)^2}. \tag{1.23}$$

It is clear that the first term in Eq.(1.23) comes from the direct response of a static cavity to the incoming field $\hat{a}_{\omega_0+\Omega}, \hat{a}^\dagger_{\omega_0-\Omega}$, which reveals the fact that the cavity field can be treated effectively map to a mechanical motion under the effect of a friction force[3]. The second term comes from the contribution of the stochastic motion of the test mass driven by the radiation pressure noise, which is equal to the transductance $Z^{\delta=0}_{+-}$ and $Z^{\delta=0}_{-+}$ when there is no detuning. Some interferometric gravitational wave detectors, such as Japanese cryogenic detector KAGRA, plan to work in the detuned region where the test masses dynamics are modified by optical spring (Aso *et al.*, 2013).

The modification of input mechanical impedance Z_{11} provides new insights about energy interactions in laser interferometers. They can be understood in a simple picture that considers only the pump beam and the sideband signals. Upper and lower sidebands are created by gravitational waves. The sidebands beat with the high power carrier light. The beating signal creates radiation pressure forces that acts on the interferometer test masses. Figure 1.33 shows the sideband energy flow. The key point is that the radiation pressure force from one sideband has the opposite phase to the force from the other sideband. Treating the gravitational wave itself as a part of the system as shown in Fig. 1.14, it follows that one sideband extracts energy from the gravitational wave, while the other sideband returns energy to the wave. Without detuning, the gravitational wave detector has zero input impedance (cf Fig. 1.19). No gravitational wave energy is absorbed. However the input impedance can be tuned to a high energy absorbing value by detuning the detector.

With appropriate parameters, detuning increases the transductance and the input impedance. Given that huge amounts of energy are available in gravitational waves, it appears self-evident that extracting more of this energy should allow substantial increases in detector sensitivity. However, to this date, it has not been proved that such configurations can increase the signal to noise ratio.

It is useful to ask what is the mechanism by which detuning increases the energy extraction? The answer is that detuning, as observed experimentally in NIOBE, creates an optical spring. A detuned interferometer ceases to be one in which test masses float freely. The optical spring creates a rigidity against which the gravitational wave has to do work. The fraction of gravitational wave energy coupled into the detector is set by the impedance mismatch ratio between the detector and the waves. While this ratio will always be tiny,due to the vast impedance c^3/G of free space to gravitational

[3]Written down explicitly, we have $\hat{A} = \sqrt{2\gamma}/(\gamma - j\Omega)\hat{a}$. This frequency domain formula corresponds to the equation of motion of intracavity field $\hat{A}$ in the time domain as $\dot{\hat{A}} = -\gamma\hat{A} + \sqrt{2\gamma}a$, which is analogous to Newton's second law: $\dot{v} = -\gamma v + f$, where v is the velocity, f and γv are respectively the driving force and friction force per unit mass.

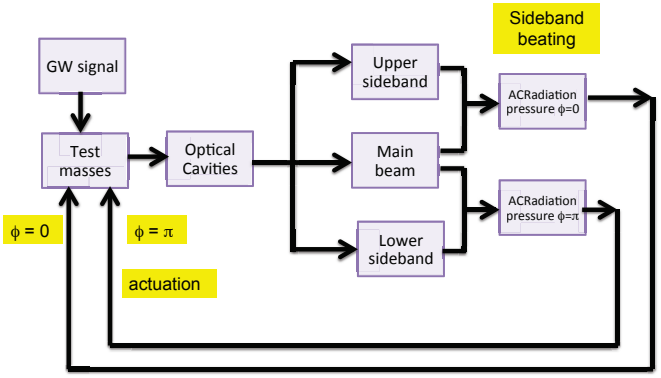

Fig. 1.33 Radiation pressure feedback in a laser interferometer. Gravitational waves create signal sidebands. Each sideband beats with the carrier creating a radiation pressure force which acts on the test masses. This radiation pressure force is either in-phase or in anti-phase. Acting together the two forces cancel so that the test mass remains as a free mass. If unbalanced the gravitational wave does work against the radiation pressure force. The radiation pressure forces determine the real and imaginary parts of the detector input impedance as we saw in sections 1.9 and 1.10. They act to change the dynamical response of the detector to gravitational waves but can also lead to instability.

waves, it is possible to increase the energy absorption by ~ 6 orders of magnitude, as shown by in (Ma *et al.*, 2015*a*) which derived the energy absorbed by the double optical spring interferometer (Rehbein *et al.*, 2008).

Modification of optomechanical dynamics not only happens for center of mass motion of test masses. It can also happen for mirror internal acoustic modes. In the next section, we will discuss this effect which is of great importance in interferometer design. We will see that the modification of the input mechanical impedance for the mirror internal acoustic modes can make it difficult to achieve the required high optical power. Solution of this problem is an important frontier of research on advanced interferometers.

1.12 Three Mode Interactions and Parametric Instability

All the parametric transducer systems discussed so far involve devices that create a pair of signal sidebands. In most devices there is an intrinsic symmetry that allows both sidebands to simultaneously exist, although their relative amplitudes can be varied by detuning.

In 2001 Braginsky et al predicted three mode interactions in which a single sideband frequency is resonant in an optical cavity transverse mode (Braginsky *et al.*, 2001). Such interactions are likely in long optical cavities because of their intrinsically asymmetric mode structure.

In the three mode interaction photons from the pump laser are scattered into transverse optical modes by acoustic modes of the mirror test masses. If the scattering transition is to a lower frequency optical mode, it creates a phonon in the test mass.

Braginsky's group showed that this interaction could generate parametric instability. Essentially it was realised that intense laser light can scatter inelastically from macroscopic acoustic modes of a mirror such that the photon energy is divided between a lower frequency transverse optical photon and an acoustic phonon in the mirror, as illustrated in Fig. 1.34(b). If the acoustic power injected by this mechanism exceeds the acoustic losses of the mirror, the mirror acoustic amplitude will grow exponentially, steadily increasing over seconds or minutes, until a very large amplitude (of say 1 nanometer) causes saturation of amplifiers and failure of the instrument.

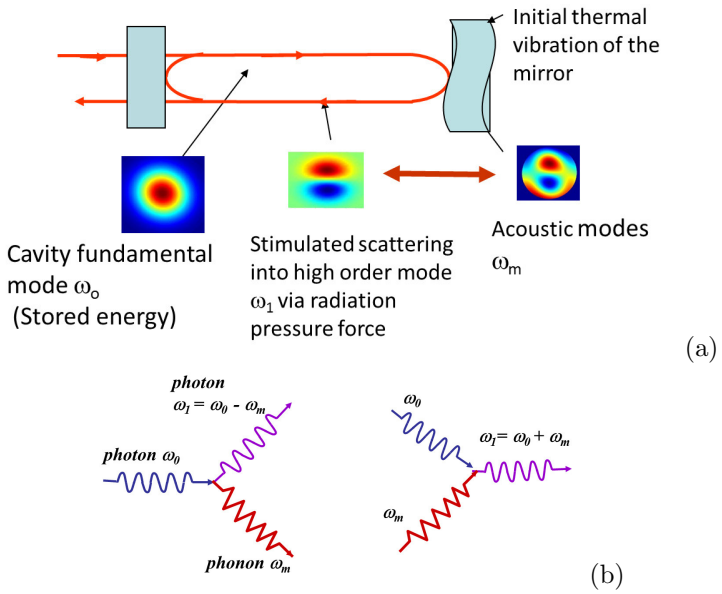

Fig. 1.34 (a) Classical picture of a cavity three-mode interaction: the main high power cavity optical mode beats with a transverse mode generated by light scattered from a mirror acoustic mode. The beat frequency causes a time varying radiation pressure force in phase with the acoustic mode. This drives the mirror and excites the acoustic mode as long as the transverse optical and acoustic mode shapes are similar. (b) The quantum picture of the three-mode parametric interaction treats it as a photon-phonon scattering process in which a carrier photon scatters from the acoustic phonon on the mirror surface to create a transverse optical mode photon. The acoustic mode frequency is exactly equal to the difference between the two optical frequencies.

In 2005 Zhao et al undertook a detailed 3D simulation of parametric instability in Advanced LIGO type detectors. This led to a prediction (Zhao *et al.*, 2005) that detectors like Advanced LIGO would indeed experience three-mode opto-mechanical instability, involving tens of acoustic modes across the four main interferometer test masses. Thereafter many sophisticated simulations and experiments in specially designed optical cavities at Gingin, Western Australia were used to study the phenomenon.

It takes the extreme technology of long baseline laser interferometers to enter the

regime where three mode instability can occur: 40kg scale mirrors with ultralow acoustic losses, 4km long optical cavities, and very high optical power $\sim$ hundreds of kilowatts. On small scales the much larger free spectral range of shorter cavities causes optical modes to be more widely spaced. Simultaneously smaller test masses have a lower acoustic mode density so that the probability of coincidences between the mode gap (the frequency difference between a cavity TEM_{00} mode and a higher order TEM_{mn} mode) and an acoustic mode becomes small. On the 80m scale of the Gingin high optical power facility (Ju *et al.*, 2004) only specific radii of curvature give conditions for instability.

Using 80m long cavities with carefully designed kg-scale test masses and high optical power it was possible to study most aspects three mode interactions: their tuning, their suppression, and their use as high sensitivity transducers for monitoring test masses.

In 2009 Zhao et al showed that 3-mode parametric interactions could be created on a table-top scale using low mass acoustic resonators in the MHz frequency range (Zhao *et al.*, 2009). A parallel program of table-top studies of three mode interactions was begun, using specially designed resonators and silicon nitride membranes. These experiments led to the first observation of three mode parametric instability in free space cavities in 2014 (Chen *et al.*, 2015).

Despite the successful creation of three mode parametric instability in a small scale device, the 2009 paper promised the creation of a new class of non-linear optomechanical parametric devices based on three mode interactions. This has not yet been realised, mainly due to the difficulty in tuning optical modes. Opto-acoustic parametric amplifiers,(Zhao *et al.*, 2009) with one acoustic channel and two optical channels offer the possibility of being general versatile devices like optical parametric amplifiers. They can allow creation of new sensors that could operate with quantum limited sensitivity,

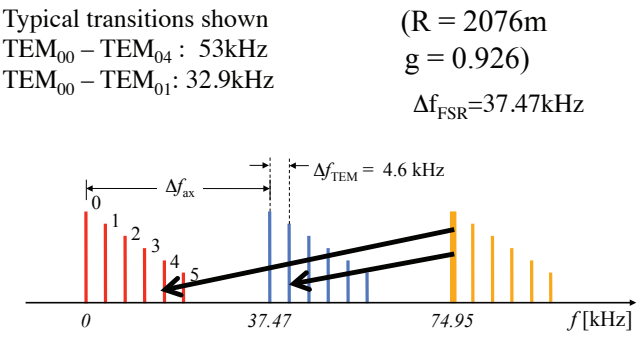

Fig. 1.35 An example of the cavity mode structure in a 4km LIGO-type arm cavity, showing the transverse mode families relative to the cavity free spectral range and typical transitions from the pump mode to certain transverse modes that could cause parametric instability if a suitable acoustic mode existed in the test mass. Because the transverse mode frequencies are strongly tuned by radius of curvature changes and typically have linewidths of kHz, the parametric gain for such transitions varies with the thermal conditions.

for the detection of weak forces and fields. Their successful implementation may need the development of other optomechanical techniques such as optical dilution discussed below.

In 2014 Zhao et al observed parametric instability in a cavity designed to be comparable to those of advanced interferometers (Zhao *et al.*, 2015). Later in 2014 the Advanced LIGO interferometer in Louisiana observed parametric instability (Evans *et al.*, 2015), at an optical power level consistent with the 2005 prediction. Preliminary estimates (Gras *et al.*, 2010) indicate that about 40 acoustic modes may be unstable in Advanced LIGO at full optical power unless control methods are implemented.

Because the frequency of transverse optical modes depends strongly on the mirror radius of curvature, any method that modifies the mirror radius of curvature can allow parametric instability to be detuned. Thermal tuning uses surface heating to change the mirror radius of curvature (by say 10m in 2000m). The method is now fully confirmed and has been used frequently at the Gingin facility to tune three mode interactions. Thermal tuning allowed the laser power threshold for instability to be raised from 5% to about 12% in the Advanced LIGO detectors (Evans *et al.*, 2015). Unfortunately in a long baseline interferometer the mode density is so high that thermal tuning generally tends to transfer the instability from one mode to another. Thus additional control techniques are required.

There are various other methods for instability control. The methods can be summarised under 4 headings (Ju *et al.*, 2009): passive damping (Gras *et al.*, 2009; Gras *et al.*, 2015), acoustic feedback(Miller *et al.*, 2011), optical feedback (Fan *et al.*, 2010; Zhang *et al.*, 2010), and detuning (Degallaix *et al.*, 2007). Keeping in mind the fact that laser interferometer gravitational wave detectors are the most sensitive instruments ever created, with displacement noise sensitivity $\sim 10^{-20}\mathrm{m}/\sqrt{\mathrm{Hz}}$, the risk in any method of instability control is that noise forces will degrade the exquisite sensitivity of the instrument. For example, noise can come from photon radiation pressure, scattered light, thermal Brownian motion, electronics noise, and inhomogeneities in mirror coatings.

Many suppression schemes such as ring dampers (Gras *et al.*, 2009) and mechanical mode dampers (Gras *et al.*, 2015) were shown by modelling to cause significant sensitivity degradation. Others such as optical feedback suppression (Fan *et al.*, 2010) were demonstrated at Gingin, but involved optical configurations that were complex and risked introduction of noise. C. Blair *et al* have shown that 15.5kHz instabilities can be controlled in LIGO by direct electrostatic feedback to the test masses using electrostatic drive plates installed in Advanced LIGO (Blair *et al.*, 2016).

In 2014 the UWA team discovered a new method (Zhao *et al.*, 2015) of suppressing instability consisting of low frequency radius of curvature modulation of test masses using modulated radiant infrared heating. Suppression is achieved by diluting the parametric gain across many modes in a time dependent fashion, using a modulation frequency below the sensitive signal band. In principle this method can suppress the parametric gain by about an order of magnitude and in theory it should not introduce significant noise.

Three mode interactions have been shown to have very high sensitivity as a readout for thermally excited acoustic modes (Ju *et al.*, 2014). Because the mode amplitude

depends strongly on three mode interaction gain conditions, simple monitoring of ultrasonic acoustic modes through their three-mode interactions can be used to predict which modes will become unstable when the power is increased. The technique was demonstrated at Gingin.

As the optical power in Advanced interferometers is stepped up, acoustic mode monitoring offers a useful tool for defining the instabilities that will have to be controlled at the next step in power. This can give enough time for suppression methods to be ready at the appropriate time. While proven at Gingin, for Advanced detectors where the ultrasonic acoustic mode density is 1000 times higher, this approach requires extensive measurements on thousands of acoustic modes, combined with detailed modelling. Reference [(Ju *et al.*, 2014)] shows that it can be developed into a powerful tool for monitoring interferometer test masses with unprecedented precision.

1.13 White Light Optomechanical Cavities for Broadband Enhancement of Gravitational Wave Detectors

We have seen above how optomechanics has been used to create gravitational wave detectors, and how three mode optomechanical interactions lead to parametric instability. In this final section we show how optomechanics can be used to create a new route to improved sensitivity, in the form of an optomechanical white light signal recycling cavity. This type of scheme has been proven theoretically (Miao *et al.*, 2015) and the associated negative dispersion have been proven in the classical regime(Qin *et al.*, 2015). The white light cavity scheme offers possibly the only possible means of significantly increasing interferometer sensitivity in a broad frequency band around 1-2kHz. However it faces formidable challenges involving beautiful new implementations of optomechanics.

Signal recycling is now a standard technique used in gravitational wave detectors to resonantly enhance the signal sidebands. Throughout physics resonance allows a narrow band of frequencies to be enhanced, at cost of reduced bandwidth. The white light cavity breaks the inverse relationship between resonant gain and bandwidth. It allows resonant build up of a broad band of frequencies. This is achieved by creating a low loss optomechanical cavity with negative dispersion that compensates the normal frequency dependence of phase accumulated in the main interferometer. The white light cavity is a cavity in which the effective light velocity depends on wavelength such that all frequencies are simultaneously resonant across the frequency band of interest.

In current advanced gravitational wave interferometers the signal recycling gain is low to prevent loss of bandwidth. White light cavities are designed to create broadband signal recycling with high gain, allowing a substantial improvement in sensitivity for signal frequencies between 200Hz and 2kHz as shown in Fig. 1.37.

The white light cavity concept was first demonstrated using atomic media (Wicht *et al.*, 2002). Research by Salit et al (Salit and Shahriar, 2010), and by Pati et al (Pati *et al.*, 2007) confirmed the concepts. However Ma et al (Ma *et al.*, 2015*b*) demonstrated that those configurations based on atomic media have fundamental noise limitations.

The breakthrough came with the recognition that the same physics can be realised with optomechanics. A millimetre scale mirror resonator coupled to a light field and pumped with blue-detuned laser light creates a cavity with negative dispersion for a

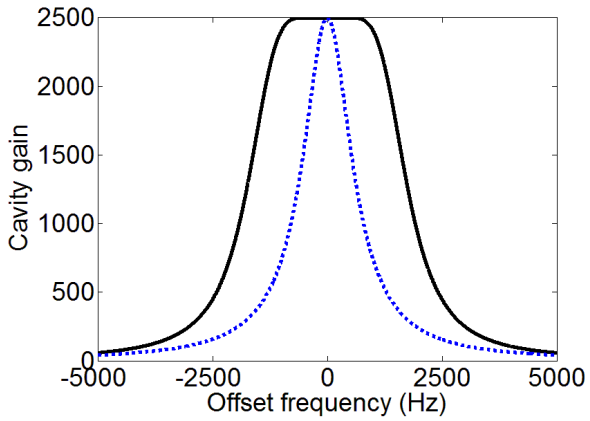

Fig. 1.36 the white light cavity frequency response (solid line) compared with that of a conventional cavity (dotted).

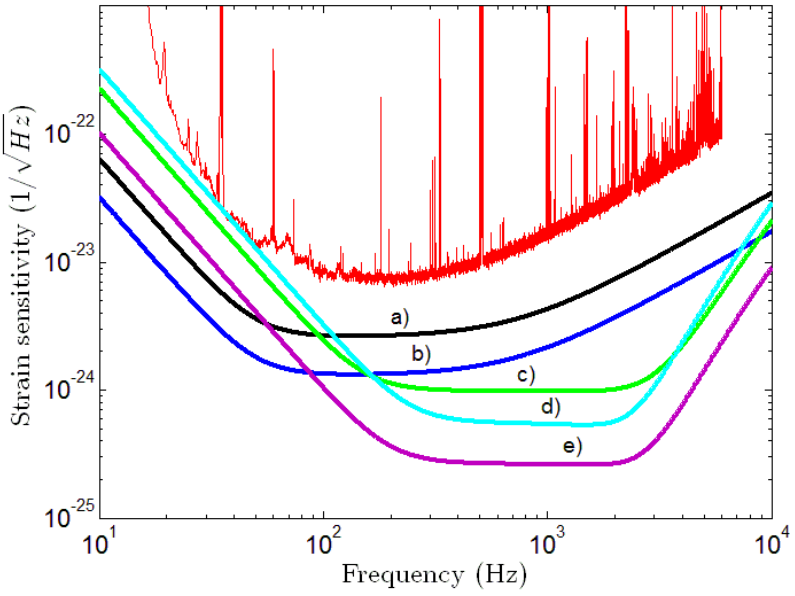

Fig. 1.37 Current Advanced LIGO sensitivity (top curve) and predicted sensitivity after a) increase of laser power to the design level, b) implementation of frequency dependent optical squeezing, c) and d) white light signal recycling at two levels of the noise parameter TQ^{-1} (see text), and e) white light signal recycling combined with frequency dependent squeezing.

signal beam, as shown in Fig. 1.38. The configuration is intrinsically unstable. The key to making it practical is to use feedback through intensity modulation of the pump beam as proposed by Miao et al (Miao *et al.*, 2015).

White light cavity technology with noise at the quantum level can increase the sensitivity of Advanced interferometers such as LIGO by 3-fold at 200Hz and 7-fold at 1-2kHz, compared with realistic estimates of the improvements already anticipated. Operated in conjunction with squeezed light techniques, white light technology could give sensitivity as shown in Fig. 1.37.

Gravitational wave event rates for binary black holes similar to the source already detected increase as the cube of the strain sensitivity in the relevant frequency band. For curve e) in Fig. 1.37 the benefits of squeezing are combined with the white light cavity. Event rates could increase to ~ 600 events per day! Other sources such 5-10 solar mass black hole binaries and the quasi-normal modes of the new born black hole could become observable within a large fraction of the observable universe.

The greatest challenge in creating a white light cavity system is in creating a suitable low optical loss resonant mirror with ultralow acoustic losses. Acoustic losses create unacceptable thermal noise and need to be reduced by a factor $\sim 10^6$. While this sounds extremely challenging, an extensive analysis and design study by Page et al (Page *et al.*, 2015) indicates that it is possible.

The attainment of minimal thermal noise at room temperature requires the combination of specially constructed resonators called cat-flap resonators, and quantum noise cancelling optical dilution systems in which the mechanical resonance is created by optical springs in a novel new cavity design called a Double End Mirror Sloshing Cavity or DEMS cavity. In the devices we propose optical dilution minimises the thermal fluctuations and optical cooling (self-cooling) suppresses the thermal amplitude.

These two techniques can allow thermal fluctuations to be suppressed below the zero-point fluctuations, thereby enabling devices that are free of thermal noise, in which the quantum behaviour of macroscopic objects can be explored. In the next paragraph we will re-visit opto-mechanical self-cooling which was already introduced in the context of NIOBE, but this time in the context of small scale resonators. Optical dilution techniques will be discussed in detail in the next section.

One of the first applications of self cooling was the cold damping of NIOBE discussed above. In 2006 Cohadon et al (Arcizet *et al.*, 2006) used optomechanics to cool a micro-resonator from 300K to 10K and suggested that optomechanical cooling to the quantum ground state might be possible. In 2011 Cohadon's prediction was realised when Chan et al (Chan *et al.*, 2011) used optomechanics to successfully cool a 3.68GHz mechanical resonator from 20K to the quantum ground state, and Teufel et al (Teufel *et al.*, 2011) used microwave optomechanics to cool a 10MHz resonator from 15mK to the ground state. This work proved that thermal-noise-free mechanical resonators were indeed attainable.

Regarding white light cavity technology, in 2014 Qin et al experimentally demonstrated (Qin *et al.*, 2015) tuneable linear negative dispersion, created in an optomechanical cavity with a blue detuned doublet of control beams. The system could have very low optical losses dominated by a few ppm optical coating loss (Rempe *et al.*, 1992).A related scheme, but using a single control beam, and feedback stabilisation,

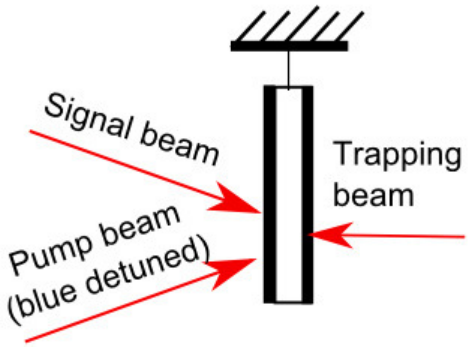

Fig. 1.38 The white light cavity (WLC) combines three laser frequencies interacting with a single high Q-factor resonator. One beam (arbitrary frequency $\sim$ 4mW) creates the optical trap which creates a mechanical resonator ($\sim$ 200kHz) with ultralow loss. The second beam (a few mW) tuned on the blue side of the optical cavity resonance creates a negative dispersion filter. The signal beam is the interferometer output signal. All beams are inside optical cavities.

was proven theoretically by Miao et al. (Miao *et al.*, 2015)

White light cavity technology opens up a broad band at the high end of the spectrum as shown in Fig. 1.37. Once brought to the quantum noise level, it could increase the sensitivity of LIGO substantially as discussed above. In the very high event rate regime, detectors could be switched between optimum high frequency sensitivity using the whilte light cavity (Fig 1.37, curves c-e), and optimum low frequency sensitivity using frequency dependent squeezing (Fig 1.37, curve b).

The lower five curves in Fig. 1.37 assume that test mass thermal noise will be suppressed by use of cryogenics,(like the Japanese detector KAGRA now under construction), silicon test masses, and low loss (low thermal noise) optical coatings such as those developed by Crystalline Mirror Systems.

The key concepts that must be implemented to attain practical white light cavity devices are summarised in Table 1.1.

1.13.1 Optical trapping, optical dilution and quantum noise

Optical traps were first used in manipulating microscopic objects such as molecules and biological cells, usually called "optical tweezers". An optical trap is a deep potential well created by radiation pressure that confines a mechanical resonator. This enables the losses to be *optically diluted*.

Using an optical trap, mechanical springs can be largely replaced by optical springs. The dilution factor is the ratio of the elastic energy stored in the optical field to the elastic energy stored in the mechanical spring. Strong optical dilution was demonstrated by Corbitt et al. (Corbitt *et al.*, 2007) who achieved a dilution factor $\sim 10^4$.

The mechanics behind optical dilution is simple. If a lossless spring $k_{\rm opt}$ is placed in parallel with a lossy spring of spring constant $k_{\rm int}$, then the Q-factor of the final resonator is given by $Q_{\rm dil} = Q_{\rm int}(k_{\rm opt}/k_{\rm int})$ assuming structural damping. Since $k \sim \omega^2$,

Table 1.1 Technical requirements for improvement of gravitational wave detectors using white light cavities.

CONCEPT	FUNCTION	BENIFIT
Optical dilution, Optical trapping	Use elastic stiffness created by radiation pressure forces to replace mechanical springs to enable thermal fluctuations to be suppressed by the ratio of optical to mechanical spring constants.	Allows creation of high frequency resonators $\sim$ 200kHz with very weak mechanical spring stiffness and very low thermal fluctuations.
Quantum noise suppression	Destructive interference of vacuum fluctuations to cancel quantum radiation pressure noise.	Create optomechanical resonators free of quantum radiation pressure noise.
Optical cooling	Extract mechanical energy from resonator.	Reduces thermal noise amplitude without cryogenic cooling.
White light cavity	Optomechanical interaction creates a negative dispersive filter. In an optical cavity a band of frequencies is simultaneously resonant.	Allows resonant enhancement of a broad band of signal frequencies in gravitational wave detectors.
Double end-mirror sloshing cavity DEMS	Cavity scheme for creating strong stable optical dilution with negative dispersion response	Allow stable operation of the system without deteriorating the signal to noise ratio.
Cat-flap Resonator	A mini-pendulum consisting of a sub-millimeter scale low loss mirror supported by a nano-scale membrane or nanowire suspension	Reduce mechanical coupling to the thermal reservoir to allow high optical dilution, in a device suitable for low loss coupling to large scale optics.

the dilution can be estimated from the square of the ratio of optical spring frequency to free resonator frequency. For maximum optical dilution we need to create resonators with the lowest possible $k_{\rm int}$ (ie the lowest possible zero-gravity frequency). In practice the quality factor of diluted resonators is less interesting than the noise. Very high Q-factors are difficult to measure and normally optical cooling will simultaneously reduce the Q-factor and the mode amplitude towards the quantum ground state.

The problems with simple optical springs are a) negative damping and b) quantum radiation pressure noise. Strong dilution requires a strong optical field acting on the mechanical resonator. By beating with vacuum fluctuations this creates strong radiation pressure noise, which drives the resonator, thereby injecting extra noise and setting limits on the maximum dilution.

In 2012 a Caltech team, led by Kimble achieved optical spring trapping in a configuration that avoided quantum radiation pressure noise (Ni *et al.*, 2012). They demonstrated optical trapping at 145kHz, and a 50-fold increase in quality factor, consistent with a prediction by Chang et al (Chang *et al.*, 2012). The mirror to flexure mass ratio limited their Q-factor, while torsional compliance and internal acoustic modes led to optically induced angular instabilities.

In 2014 Ma et al (Ma *et al.*, 2014) and Miao et al (Miao *et al.*, 2015) analyzed alternative dilution schemes; one in which the resonator mirror sits in the middle of an optical cavity, the other an optomechanical cavity with double optical spring. It was shown that a high reflectivity end mirror enables total destructive quantum interference to cancel the radiation pressure noise (Marquardt *et al.*, 2009), while instabilities from negative damping are canceled.

The Double End Mirror Sloshing Cavity or DEMS cavity is topologically equivalent to the membrane in the middle cavity. Figure 1.41 shows the DEMS cavity design. It has the same Hamiltonian, the same noise cancellation and allows use of a double sided high reflectivity cat-flap resonator (see Fig. 1.39. The DEMS cavity creates optical springs in such a way that the negative damping terms cancel, to prevent spring instabilities and also allows quantum radiation pressure noise to be suppressed (Ma *et al.*, 2014; Page *et al.*, 2015). Note that the DEMS configuration mirror-in-the-middle configuration are equivalent. The former allows separate control of transmission and reflectivity and allows for use of an opaque substrate.

The key to creating ultra-high Q-factors is to create resonators with minimal surface density, low acoustic loss suspensions. Reference [Page *et al.* 2015] shows that dilution factors of $10^8 - 10^{12}$ can be achieved in cat-flap resonators , that utilise thin suspension elements and adequate low loss materials as discussed below.

1.13.2 Optomechanical devices for gravitational wave detectors

While experiments on optomechanical devices have proved that the quantum ground state is attainable, this has only been attained under special conditions of very low mass, high mechanical frequency and cryogenic cooling. See the 2014 review by Aspelmeyer et al. (Aspelmeyer *et al.*, 2014). Devices suitable for enhancing gravitational wave detectors have not yet been developed. They must have low optical losses and ideally should operate at room temperature, but should have mechanical noise close to the quantum ground state, therefore requiring optical cooling.

Aspelmeyer et al (Aspelmeyer *et al.*, 2014) pointed out that the minimum requirement for quantum optomechanics at room temperature is the product of Q-factor $\times$ frequency $> 6 \times 10^{12}$. Optomechanical devices for enhancing gravitational wave detectors have additional requirements which have not been met in any devices to date. The requirement is determined by the detector bandwidth and leads to even higher Q-factor requirements. Figure 1.39 shows the gain improvement ratio at 2 kHz as a function of resonator Q-factor. This shows that Q-factors must be in the range $10^{10} - 10^{12}$ (Miao *et al.*, 2015) to achieve up to 7-fold improvement in detector sensitivity.

The cat-flap resonator: The cat-flap is a miniature flexure pendulum with a flat square optical test mass with linear dimension between 1mm and 0.1mm. Current devices use a silicon nitride membrane or nanowires as the flexure. Future devices could

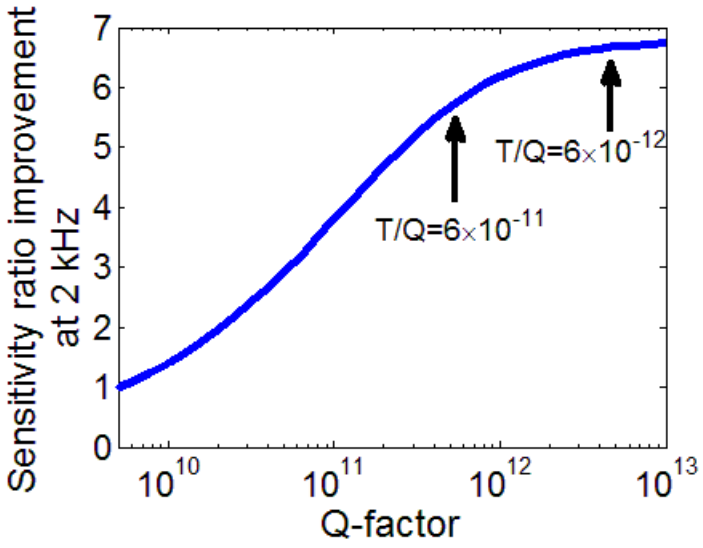

Fig. 1.39 The gain improvement ratio at 2 kHz detection frequency as a function of resonator Q-factor.

use graphene or nanotube suspensions. Optical dilution can allow extraordinarily high quality factors, limited by two main loss mechanisms as discussed below.

a) Acceleration loss: the optical force from the optical spring acting mainly on the mirror surface, deforms the mirror as it accelerates, thereby coupling the resonator to internal loss mechanisms. This loss reduces as $(\omega_{\rm int}/\omega_{\rm opt})^2$, thus requiring the resonator to be small and $\omega_{\rm opt}$ not to be too high.

b) Suspension losses. These are mainly due to violin string modes in the suspension fibres and require very high tension in low mass density suspensions. This limits the maximum length of the suspension fibre to keep violin string frequencies $>$ 1MHz. Centre of percussion tuning of the trapped resonator by adjusting the laser spot position, can be used to reduce suspension losses 3-fold by ensuring that translational reaction forces do not act at the suspension point, as demonstrated by Braginsky et al (Braginsky *et al.*, 1999).

Silicon nitride flexures can be constructed in the $10-50$ nm thickness range. Since the flexure spring constant depends on the cube of the flexure thickness/length ratio there is large benefit in minimising the thickness. The suspension materials have high tensile strength. We have designed for safety factors ~ 5. SiN tensile membranes show $Q \sim 5\times10^7$ (Chakram *et al.*, 2014) at room temperature. For our design the internal membrane modes are about 10-times higher than the resonator frequency to reduce the acceleration loss due to the coupling between the optical spring and the mirror internal modes. Smaller resonators can also be suspended with silicon nitride nanowires.

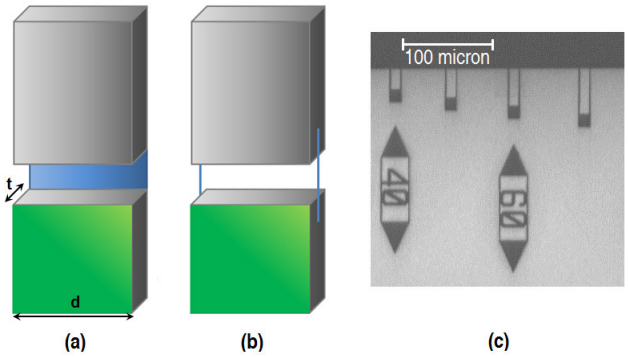

Fig. 1.40 The cat-flap resonator: A 0.5mm × 0.5mm low loss mirror suspended by a) a 10-50nm silicon nitride membrane, b), two nanowires, c) image of subscale devices created by TNO.

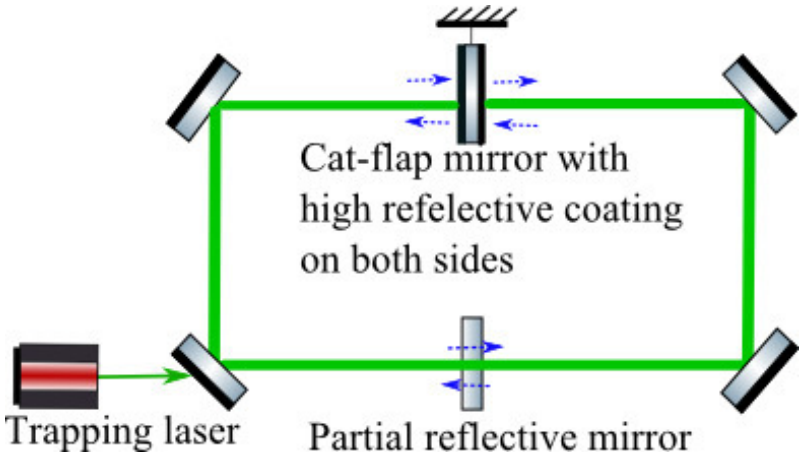

Fig. 1.41 The Double End-Mirror Sloshing (DEMS) cavity, that applies optical spring forces to trap the cat-flap resonator while suppressing quantum noise through interference. The two surfaces of the cat-flap mirror are the end mirrors of a two mode Fabry-Perot cavity. The tow modes are created by the partially reflective mirror.

The intrinsic (gravity-free) frequency of the silicon nitride cat-flap is $\sim$ 20Hz. If this is diluted to 200kHz we have typical dilution factors of $\sim 10^8$. The Q-enhancement will be less than the dilution factor due to the loss mechanisms discussed above. We estimate that $Q \sim 10^{11}$ could be observable at 200kHz for a 0.5mm square and 0.1mm thick resonator.

1.14 Conclusion

We have surveyed concepts of optomechanics from the first implementation of superconducting parametric transducers to current research challenges aiming to create

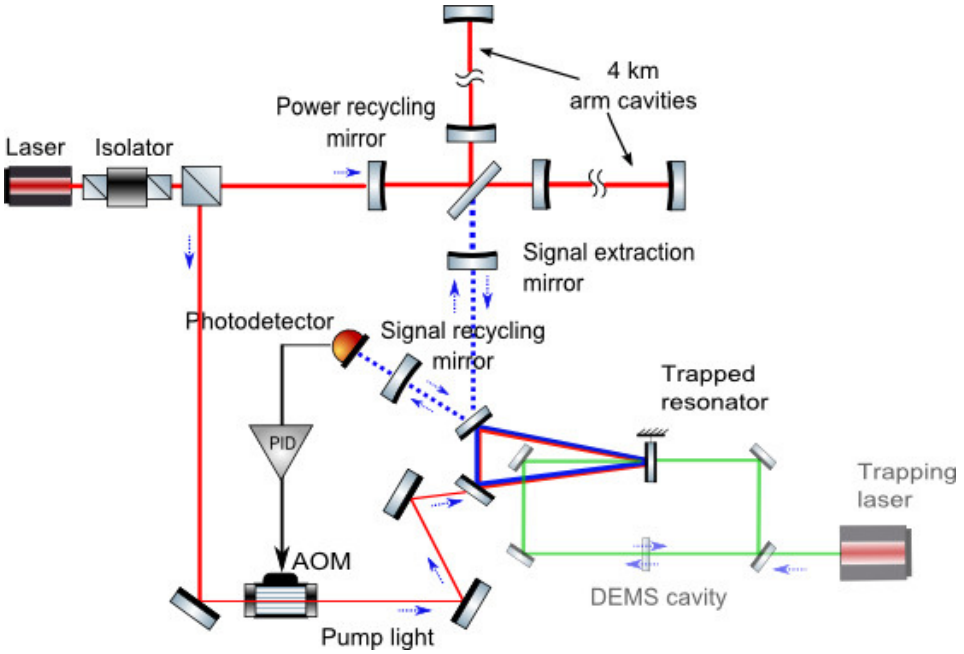

Fig. 1.42 Laser interferometer gravitational wave detector with a white light cavity signal recycling cavity. Negative dispersion is created in the triangular dispersion cavity. This acts as a dispersive mirror, changing the length of the dotted optical path. The optically trapped resonator in Fig. 1.41 is the key component in the negative dispersion cavity, which is activated through injection of blue detuned pump light. Feedback forces are applied by intensity modulation of the pump light using an acousto-optic modulator (AOM).

optomechanical devices at room temperature that are largely free of thermal noise. In between we reviewed the analysis of parametric transducers that first predicted interesting resolved sideband phenomena and the nulling of the mechanical input impedance. We went on to examine the use of microwave re-entrant cavity transducers and their application on the detector NIOBE which was an extreme large scale application of optomechanics using microwaves. This experiment demonstrated strong self damping and strong optical springs. Then we went on to examine the same physics applied to laser interferometer gravitational wave detectors and the optomechanics of three mode interactions which are a significant instability mechanism in the current advanced gravitational wave detectors. The final section described a broad research program now underway aiming to create noise free optomechanical devices suitable for low loss light processing, able to create long white light cavities. While our focus has been in improving gravitational wave detectors, optical dilution has the possibility of broad applications from macroscopic quantum mechanics two new ultra-high devices for measuring forces and fields.

References

Aasi, J. *et. al.* (2015). Advanced ligo. *Classical and Quantum Gravity*, **32**(7), 074001.

Abbott, B. P. *et. al.* (2016). Observation of gravitational waves from a binary black hole merger. *Phys. Rev. Lett.*, **116**, 061102.

Ade, P. A. R., Aghanim, N., and Ahmed, Z. *et.al.* (2015, Mar). Joint analysis of bicep2/ *Keck Array* and *Planck* data. *Phys. Rev. Lett.*, **114**, 101301.

Allen, Z. A., Astone, P., and Baggio, L. *et. al.* (2000, Dec). First search for gravitational wave bursts with a network of detectors. *Phys. Rev. Lett.*, **85**, 5046–5050.

Arcizet, O., Cohadon, P.-F., Briant, T., Pinard, M., and Heidmann, A. (2006). Radiation-pressure cooling and optomechanical instability of a micromirror. *Nature*, **444**, 71–74.

Aso, Y., Michimura, Y., Somiya, K., Ando, M., Miyakawa, O., Sekiguchi, T., Tatsumi, D., and Yamamoto, H. (2013). Interferometer design of the kagra gravitational wave detector. *Phys. Rev. D*, **88**(043007).

Aspelmeyer, M., Kippenberg, T. J., and Marquardt, F. (2014, Dec). Cavity optomechanics. *Rev. Mod. Phys.*, **86**, 1391–1452.

Blair, C., Zhao, C., Liu, J., Blair, D., Betzwieser, J., Frolov, V., DeRossa, R., Adams, C., OReilly, B., Lormand, M, Grote, H., Miller, J., Fritschel, P., Gras, S., and Evans, M. (2016). First demonstration of electrostatic damping of parametric instability at advanced ligo. *LIGO Doc P1600090-v4*.

Blair, D., Howell, E., Ju, L., and Zhao, C. (2012). *Advanced Gravitational Wave Detectors*. Cambridge Unv. Pess.

Blair, D. G. (1979). Superconducting accelerometer using niobiumonsapphire rf resonator. *Review of Scientific Instruments*, **50**(3).

Blair, D. G. (1980). Gravity wave antenna-transducer systems in gravitational radiation. In *Collapsed Objects and Exact Solutions, Ed C Edwards, Lecture Notes in Physics*, Volume 124, p. 299. Springer-Verlag, Birlin.

Blair, D. G., Bermat, T. P., and Hamilton, W O (1975). Superconducting accelerometer for use in gravity wave experiment. In *Proceedings of the 14th International Conference on Low Temperature Physics*, Volume 50, pp. 254–257. North-Holland.

Blair, D. G., Giles, A., and Zeng, M. (1987). Impedance matching element for a gravitational radiation detector. *Journal of Physics D: Applied Physics*, **20**(2), 162.

Blair, D. G. and Hamilton, W. O. (1979). Fabrication and properties of rf niobiumonsapphire superconducting resonators. *Review of Scientific Instruments*, **50**(3).

Blair, D. G., Ivanov, E. N., Tobar, M. E., Turner, P. J., van Kann, F., and Heng, I. S. (1995). High sensitivity gravitational wave antenna with parametric transducer readout. *Phys. Rev. Lett.*, **74**, 1908–1911.

Blair, D. G. and Mann, A. G. (1981). Low-noise temperature gravitational-radiation antenna-transducer system. *Nuovo Cimento B*, **61B**(1), 73–81.

Boughn, S., Fairbank, W. M., McAshan, M., Paik, H. J., Taber, R. C., Bernat, T. P., Blair, D. G., and Hamilton, W. O. (1974). The use of cryogenic technique to achieve high sensitivity in gravitational wave detectors. In *Proc. of the IAU. Conference on Gravitational Radiation and Gravitational Collapse*, Volume 64, pp. 40–51. Reidel. 1973 Warsaw, Poland.

Braginsky, V. B., Levin, Yu., and Vyatchanin, S. P. (1999). How to reduce suspension thermal noise in ligo without improving the Q of the pendulum and violin modes. *Measurement Science and Technology*, **10**(7), 598.

Braginsky, V. B., Strigin, S.E., and Vyatchanin, S.P. (2001). Parametric oscillatory instability in fabry-perot interferometer. *Phys. Lett. A*, **287**, 331.

Braginsky, V. B., Vorontsov, Yu. I., and Khalili, F. Ya. (1978). Optimal quantum measurements in gravitational-wave detectors. *Sov. Phys. JETP*, **27**, 276.

Buonanno, A. and Chen, Y. (2003, Jan). Scaling law in signal recycled laser-interferometer gravitational-wave detectors. *Phys. Rev. D*, **67**, 062002.

Chakram, S., Patil, Y. S., Chang, L., and Vengalattore, M. (2014, Mar). Dissipation in ultrahigh quality factor sin membrane resonators. *Phys. Rev. Lett.*, **112**, 127201.

Chan, J., Alegre, T. P. M., Safavi-Naeini, A. H., Hill, J. T., Krause, A., Gröblacher, S., Aspelmeyer, M., and Painter, O. (2011). Laser cooling of a nanomechanical oscillator into its quantum ground state. *Nature*, **478**, 89–92.

Chang, D. E., Ni, K. K., Painter, O., and Kimble, H. J. (2012). Ultrahigh- Q mechanical oscillators through optical trapping. *New Journal of Physics*, **14**(4), 045002.

Chen, X., Zhao, C., Danilishin, S., Ju, L., Blair, D., Wang, H., Vyatchanin, S. P., Molinelli, C., Kuhn, A., Gras, S., Briant, T., Cohadon, P. F., Heidmann, A., Roch-Jeune, I., Flaminio, R., Michel, C., and Pinard, L. (2015, Mar). Observation of three-mode parametric instability. *Phys. Rev. A*, **91**, 033832.

Corbitt, T., Chen, Y., Khalili, F., D. Ottaway, S. Vyatchanin, Whitcomb, S., and Mavalvala, N. (2006). Squeezed-state source using radiation-pressure-induced rigidity. *Phys.Rev.A*, **73**(023801).

Corbitt, T., Wipf, C., Bodiya, T., Ottaway, D., Sigg, D., Smith, N., Whitcomb, S., and Mavalvala, N. (2007, Oct). Optical dilution and feedback cooling of a gram-scale oscillator to 6.9 mk. *Phys. Rev. Lett.*, **99**, 160801.

Cuthbertson, B. D., Tobar, M. E., Ivanov, E. N., and Blair, D. G. (1998). Sensitivity and optimization of a high-q sapphire dielectric motion- sensing transducer. *IEEE Transactions on Ultrasonics, Ferroelectrics, and Frequency control*, **45**(5), 1303.

Degallaix, J., Zhao, C., Ju, L., and Blair, D. G. (2007, Jun). Thermal tuning of optical cavities for parametric instability control. *J. Opt. Soc. Am. B*, **24**(6), 1336–1343.

Drever, R. W. P., Hough, J., Munley, A. J., Lee, S. A., Spero, R. E., Whitcomb, S. E., Ward, H., Ford, G. M., Hereld, M., Robertson, N. A., Kerr, I., Pugh, J. R., Newton, G. P., Meers, B. J., Brooks III, E. D., and Grsel, Y. (1981). Gravitational wave detectors using laser interferometers and optical cavities: Ideas, principles and prospects. In *Quantum Optics, Experimental Gravity, and Measurement Theory, Proceedings of the NATO Advanced Study Institute, NATO ASI Series B, (Plenum Press, New York, 1983).*, p. 503514 vol.94.

Einstein, A. (1916, June). Näherungsweise integration der feldgleichungen der gravitation. *Sitzungsberichte der Königlich Preussischen Akademie der Wissenschaften*

Berlin, **part 1:**, 688C696.

Einstein, A. (1918, June). Näherungsweise integration der feldgleichungen der gravitation. *Sitzungsberichte der Königlich Preussischen Akademie der Wissenschaften Berlin*, **part 2:**, 154C167.

Evans, M., Gras, S., and Fritschel, P. *et. al.* (2015, Apr). Observation of parametric instability in advanced ligo. *Phys. Rev. Lett.*, **114**, 161102.

Fan, Y., Merrill, L., Zhao, C., Ju, Li, Blair, D., Slagmolen, B., Hosken, D., Brooks, A., Veitch, P., and Munch, J. (2010). Testing the suppression of opto-acoustic parametric interactions using optical feedback control. *Classical and Quantum Gravity*, **27**(8), 084028.

Giffard, R. P. (1976, Nov). Ultimate sensitivity limit of a resonant gravitational wave antenna using a linear motion detector. *Phys. Rev. D*, **14**, 2478–2486.

Gras, S., Blair, D. G., and Zhao, C. (2009). Suppression of parametric instabilities in future gravitational wave detectors using damping rings. *Classical and Quantum Gravity*, **26**(13), 135012.

Gras, S., Fritschel, P., Barsotti, L., and Evans, M. (2015, Oct). Resonant dampers for parametric instabilities in gravitational wave detectors. *Phys. Rev. D*, **92**, 082001.

Gras, S., Zhao, C., Blair, D. G., and Ju, L. (2010). Parametric instabilities in advanced gravitational wave detectors. *Classical and Quantum Gravity*, **27**(20), 205019.

Heffner, H. (1962, July). The fundamental noise limit of linear amplifiers. In *Proceedings of the IRE*, Volume 50, pp. 1604 – 1608.

Hertz, H. R. (1887, May). über sehr schnelle electrische schwingungen. *Annalen der Physik*, **267**(7), 421C44.

Ivanov, E. N., Turner, P. J., and Blair, D. G. (1993). Microwave signal processing for a cryogenic gravitational radiation antenna with a noncontacting readout. *Review of Scientific Instruments*, **64**(11).

Ju, L., Aoun, M., and *et.al*, P. Barriga (2004). ACIGA's high optical power test facility. *Classical and Quantum Gravity*, **21**(5), S887.

Ju, L., Blair, D. G., Zhao, C., Gras, S., Zhang, Z., Barriga, P., Miao, H., Fan, Y., and Merrill, L. (2009). Strategies for the control of parametric instability in advanced gravitational wave detectors. *Classical and Quantum Gravity*, **26**(1), 015002.

Ju, L., Zhao, C, Blair, D. G., Gras, S., Susmithan, S., Fang, Q., and Blair, C. D. (2014). Three mode interactions as a precision monitoring tool for advanced laser interferometers. *Classical and Quantum Gravity*, **31**(18), 185003.

Kimble, H. J., Levin, Yuri, Matsko, Andrey B., Thorne, Kip S., and Vyatchanin, Sergey P. (2001). Conversion of conventional gravitational-wave interferometers into quantum nondemolition interferometers by modifying their input and/or output optics. *Phys. Rev. D 65, 022002,(2001)*, **65**(022002).

Ma, Y., Blair, D. G., C, Zhao., and Kells, W. (2015*a*). Extraction of energy from gravitational waves by laser interferometer detectors. *Classical and Quantum Gravity*, **32**(1), 015003.

Ma, Y., Danilishin, S. L., Zhao, C., Miao, H., Korth, W. Z., Chen, Y., Ward, R. L., and Blair, D. G. (2014, Oct). Narrowing the filter-cavity bandwidth in gravitational-wave detectors via optomechanical interaction. *Phys. Rev. Lett.*, **113**, 151102.

Ma, Y., Miao, H., Zhao, C., and Chen, Y. (2015*b*, Aug). Quantum noise of a white-light cavity using a double-pumped gain medium. *Phys. Rev. A*, **92**, 023807.

Manley, J. M. and Rowe, H. E. (1956, July). Some general properties of nonlinear elements-part i. general energy relations. *Proceedings of the IRE*, **44**(7), 904–913.

Marquardt, F., Girvin, S. M., and Clerk, A. A. (2009, May). Quantum noise interference and backaction cooling in cavity nanomechanics. *Phys. Rev. Lett.*, **102**, 207209.

Maxwell, J. C. (1865, June). A dynamical theory of the electromagnetic field. *Transactions of the Royal Society*, **June 15**.

Meers, B. J. (1988, Oct). Recycling in laser-interferometric gravitational-wave detectors. *Phys. Rev. D*, **38**, 2317–2326.

Miao, H., Ma, Y., Zhao, C., and Chen, Y. (2015, Nov). Enhancing the bandwidth of gravitational-wave detectors with unstable optomechanical filters. *Phys. Rev. Lett.*, **115**, 211104.

Miller, J., Evans, M., Barsotti, L., Fritschel, P., MacInnis, M., Mittleman, R., Shapiro, B., Soto, J., and Torrie, C. (2011). Damping parametric instabilities in future gravitational wave detectors by means of electrostatic actuators. *Physics Letters A*, **375**(3), 788 – 794.

Ni, K.-K., Norte, R., Wilson, D. J., Hood, J. D., Chang, D. E., Painter, O., and Kimble, H. J. (2012, May). Enhancement of mechanical Q factors by optical trapping. *Phys. Rev. Lett.*, **108**, 214302.

Page, M., Ma, Y., Zhao, C., Blair, D., Ju, L., Pan, H-W., Chao, S., Mitrofanov, V., and Sadeghian, H. (2015). Thermal noise free opto-mechanics using strong optical springs.

Paik, H. J. (1976). Superconducting tunable-?diaphragm transducer for sensitive acceleration measurements. *Journal of Applied Physics*, **47**(3).

Pati, G. S., Salit, M., Salit, K., and Shahriar, M. S. (2007, Sep). Demonstration of a tunable-bandwidth white-light interferometer using anomalous dispersion in atomic vapor. *Phys. Rev. Lett.*, **99**, 133601.

Peng, H. and Blair, D. G. (1994). Test of an interferometric sapphire transducer with the super attenuator of the virgo gravitational wave antenna. *Phys. Lett. A*, **189**(5), 141–144.

Peng, H., Blair, D. G., and Ivanov, E. N. (1994). An ultra high sensitivity transducer for vibration measurement. *J. Phys. D: Appl. Phys.*, **27**, 1150–1155.

Press, W. H. and Teukolsdy, S. A. (1977). On formation of close binaries by 2-body tidal capture. *Astrophys. J.*, **213**(17), 183–192.

Pretorius, F. (2005, Sep). Evolution of binary black-hole spacetimes. *Phys. Rev. Lett.*, **95**, 121101.

Purdy, T. P., Yu, P.-L., Peterson, R. W., Kampel, N. S., and Regal, C. A. (2013). Strong optomechanical squeezing of light. *Phys.Rev.X*, **3**(031012).

Qin, J., Zhao, C., Ma, Y., Ju, L., and Blair, D. G. (2015, May). Linear negative dispersion with a gain doublet via optomechanical interactions. *Opt. Lett.*, **40**(10), 2337–2340.

Rehbein, H., Müller-Ebhardt, H., Somiya, K., Danilishin, S. L., Schnabel, R., Danzmann, K., and Chen, Y. (2008, Sep). Double optical spring enhancement for

gravitational-wave detectors. *Phys. Rev. D*, **78**, 062003.

Rempe, G., Lalezari, R., Thompson, R. J., and Kimble, H. J. (1992, Mar). Measurement of ultralow losses in an optical interferometer. *Opt. Lett.*, **17**(5), 363–365.

Rickles, D. and DeWitt, C. M. (2011). The role of gravitation in physics, report from the 1957 chapel hill conference. *Edition Open Access*, **source 5**.

Salit, M. and Shahriar, M. S. (2010). Enhancement of sensitivity and bandwidth of gravitational wave detectors using fast-light-based white light cavities. *Journal of Optics*, **12**(10), 104014.

Teufel, J. D., Donner, T., Li, Dale, Harlow, J. W., Allman, M. S., Cicak, K., Sirois, A. J., Whittaker, J. D., Lehnert, K. W., and Simmonds, R. W. (2011). Sideband cooling of micromechanical motion to the quantum ground state. *Nature*, **475**, 359–363.

et.al., J. Abadie (2010). Predictions for the rates of compact binary coalescences observable by ground-based gravitational-wave detectors. *Classical and Quantum Gravity*, **27**(17), 173001.

Tobar, M. E. and Blair, D. G. (1992, June). Phase noise of a tunable and fixed frequency sapphire loaded superconducting cavity oscillator. In *Microwave Symposium Digest, 1992., IEEE MTT-S International*, pp. 477–480 vol.1.

Underwood, M., Mason, D., Lee, D., Xu, H., Jiang, L., Shkarin, A. B., Børkje, K., Girvin, S. M., and Harris, J. G. E. (2015, Dec). Measurement of the motional sidebands of a nanogram-scale oscillator in the quantum regime. *Phys. Rev. A*, **92**, 061801.

Weber, J. (1960, Janunary). Detection and generation of gravitational waves. *Phys. Rev.*, **117**(1), 306.

Weber, J. (1961). *General Relativity and Gravitational Waves*. Wiley-Interscience, New York.

Weber, J. (1970, Jul). Anisotropy and polarization in the gravitational-radiation experiments. *Phys. Rev. Lett.*, **25**, 180–184.

Weber, J., Lee, M., Gretz, D. J., Rydbeck, G., Trimble, V. L., and Steppel, S. (1973, Sep). New gravitational radiation experiments. *Phys. Rev. Lett.*, **31**, 779–783.

Wicht, A., Rinkleff, R.-H., Spani Molella, L., and Danzmann, K. (2002, Dec). Comparative study of anomalous dispersive transparent media. *Phys. Rev. A*, **66**, 063815.

Zhang, Z., Zhao, C., Ju, L., and Blair, D. G. (2010, Jan). Enhancement and suppression of opto-acoustic parametric interactions using optical feedback. *Phys. Rev. A*, **81**, 013822.

Zhao, C., Ju, L., Degallaix, J., Gras, S., and Blair, D. G. (2005, Apr). Parametric instabilities and their control in advanced interferometer gravitational-wave detectors. *Phys. Rev. Lett.*, **94**, 121102.

Zhao, C., Ju, L., Fang, Q., Blair, C., Qin, J., Blair, D. G., Degallaix, J., and Yamamoto, H. (2015, May). Parametric instability in long optical cavities and suppression by dynamic transverse mode frequency modulation. *Phys. Rev. D*, **91**, 092001.

Zhao, C., Ju, L., Miao, H., Gras, S., Fan, Y., and Blair, D. G. (2009, Jun). Three-mode optoacoustic parametric amplifier: A tool for macroscopic quantum experiments. *Phys. Rev. Lett.*, **102**, 243902.